11-12-2009

Development and Deployment of an Underwater Mass Spectrometer for Quantitative Measurements of Dissolved Gases

Ryan J. Bell
University of South Florida

Development and Deployment of an Underwater Mass Spectrometer for Quantitative Measurements of Dissolved Gases

by

Ryan J. Bell

A dissertation submitted in partial fulfillment
of the requirements for the degree of
Doctor of Philosophy
College of Marine Science
University of South Florida

Major Professor: Robert H. Byrne, Ph.D.
Robert T. Short, Ph.D.
Edward S. Van Vleet, Ph.D.
Frants R. Lauritsen, Ph.D.
Friso H.W. van Amerom, Ph.D.
Luis H. Garcia-Rubio, Ph.D.

Date of Approval:
November 12, 2009

Keywords: membrane inlet mass spectrometry, seawater chemistry, polydimethylsiloxane permeability, sediment porewater, carbon dioxide

Dedication

To Carrie.

Acknowledgments

I express my deep appreciation to my major academic advisor, Dr. Robert Byrne. His patience, guidance, and confidence in my abilities have enabled my academic development and success while his dedication and openness have made my tenure at the University of South Florida a positive experience.

Without the encouragement, guidance and support of Dr. Robert T. Short, the success of this work would not have been possible. The opportunities Dr. Short has afforded me through my employment at the Center for Ocean Technology and SRI International have been and will continue to be indispensable throughout my professional development.

I would also like to express my appreciation to committee members Dr. Edward Van Vleet, Dr. Frants Lauritsen, Dr. Friso van Amerom, and Dr. Luis Garcia-Rubio for their indispensible critical reviews and valuable discussions.

A special thank you goes to the past and present members of our research group: Dr. Friso van Amerom, Dr. Strawn Toler, Peter Wenner, Gottfried Kibelka, Dr. Andres Cardenas, John Edkins, Karsten Köhn, Luis Miranda, Matthias Elliott, Sandra Gassig, Julie Pierce, Jeremy Fowers and Mauricio Lanio. Their advice and friendship have contributed immeasurably to my personal and academic development. Without their direction and support, none of this work would have been possible.

I thank Dr. Lori Adornato, Gottfried Kibelka, Dr. Xuewu Liu, and Dr. William Savidge for their critical discussions and focused comments that kept this work sound and accurate, while expanding its scientific relevance.

I gratefully acknowledge the contributions from technical collaborators: Joe Kolesar for his unending willingness to help (and his lively debates); Ray Hazen for the electrical engineering mentoring, for which I am tremendously indebted; Mike Hall and William Huzar for enduring the endless modification requests; and Bill Range for his anecdotes and grammar lessons.

I thank the staff and crew of the R/V Bellows, R/V Suncoaster, R/V Savannah, and R/V Pelican who enabled the collection of much of the data presented here.

I would like to express my gratitude to my parents, Tom and Nancy Bell; my brother, Sean; and my Gramma, Agnes Jefferson, for their unending love and support through every phase of my life. My deepest thanks go to Carrie Wall for her support and devotion in times of need, and her humor and love in times of elation. Carrie's help collecting samples and making edits in the wee hours is much appreciated, and her support is everything to me. Lastly, I thank our blind cavefish for inspiring me with daily demonstrations of Mother Nature's incredible accomplishments in underwater chemical sensing.

Note to Reader

Note to Reader: The original of this document contains color that is necessary for understanding the data. The original dissertation is on file with the USF library in Tampa, Florida.

Table of Contents

List of Tables

List of Figures

Development and Deployment of an Underwater Mass Spectrometer for Quantitative Measurements of Dissolved Gases

Ryan J. Bell

ABSTRACT

Manual collection and processing of seawater samples for dissolved gas analyses are technically challenging, time consuming and costly. Accordingly, in situ analysis techniques present attractive alternatives to conventional gas measurement procedures. To meet the demands of sustained, high-resolution chemical observations of the oceans, the University of South Florida and SRI International developed underwater mass spectrometer systems for quantitative measurements of dissolved gases and volatile organic compounds. This work describes the influence of variable in situ conditions on the performance of a membrane introduction mass spectrometer used for measurements in both the water column and sediment porewater.

Laboratory experiments to simulate the effects of field conditions on the membrane were performed by varying sample flow rate, salinity, hydrostatic pressure, and chemistry. Data indicate that membrane permeability has a strong dependence on hydrostatic pressure, and a weak dependence on salinity. Under slow flow conditions bicarbonates in solution contributed to carbon dioxide instrument response as a result of carbon system equilibration processes in the boundary layer at the membrane interface. In addition, method development was undertaken to enable underwater sediment porewater analyses and quantitative (calibrated) measurements of total dissolved

inorganic carbon (DIC). This work establishes the capability of membrane introduction mass spectrometry to measure two compatible variables (DIC and dissolved CO_2) for comprehensive CO_2-system characterizations.

In addition to laboratory studies three types of field observation were obtained in this work. High-resolution vertical profiles of dissolved gases in the Gulf of Mexico were obtained through system calibration and characterization of the influence of hydrostatic pressure on the behavior of polydimethylsiloxane membranes. In the South Atlantic Bight, sediment porewater profiles of dissolved gases were repeatedly obtained over a 54 hr period. Data trends were in agreement with high remineralization rates facilitated by porewater advection. Finally, time-series underwater DIC measurements that were undertaken proved to be in good accord with results obtained using conventional techniques. These measurements constitute the first quantitative observations of dissolved gas ocean profiles, sediment porewater profiles, and DIC measurements by underwater mass spectrometry.

Chapter 1: Introduction

Modern mass spectrometers have an extraordinarily wide range of analytical capabilities including isotopic ratios determinations, ultra-trace analyte detection, and large molecule fingerprinting (Hoffmann and Stroobant, 2007). Even simple systems such as membrane inlet mass spectrometers (MIMS) are able to simultaneously quantify multiple analytes over a wide dynamic range (Ketola et al., 1997). As MIMS systems require no reagent or sample preparation for analyses of gaseous or aqueous gas samples, they are easily configured for work in the field, including in situ analysis. Field portable instrumentation is advantageous because it provides for adaptive analysis, enhances spatial and temporal coverage, and reduces the likelihood of contamination during sample collection and handling. MIMS analytes have ranged from simple gases such as hydrogen, methane, dinitrogen, nitrous oxide, oxygen, hydrogen sulfide, argon, and carbon dioxide to volatile organic compounds such as dimethyl sulfide, chloroform, benzene, and toluene (LaPack, 1995; Lennemann, 1999; Bell et al., 2004). Methodologies for portable MIMS systems have been developed for semi-volatile compounds (Matz et al., 1999), and capabilities for accurate isotope ratio measurements are emerging (Camilli and Duryea, 2009; Kibelka et al., 2009).

Development of underwater mass spectrometry at the University of South Florida (Center for Ocean Technology) and SRI International has focused on the use of MIMS systems for in situ applications (Short et al., 1999) (see Appendix 1 for specifications and system level design). Measurement accuracy is a significant issue for in situ MIMS

measurements because instrument signal intensity, which is dependent on analyte concentration gradients across a gas-permeable membrane, is affected by two phenomena; a) development of a depleted boundary layer at the membrane surface and b) changes in membrane permeability that result from changes in hydrostatic pressure, temperature, and salinity. The central goal of this dissertation was to quantitatively characterize the extent to which various parameters influence the response of underwater MIMS instrumentation, and thereby to expand the instrumental capabilities and applications of MIMS for analysis of seawater and other natural solutions.

In situ MIMS measurements at full ocean depths require characterization of the influence of hydrostatic pressure on the permeability of MIMS inlet systems. Chapter 2 addresses the effect of hydrostatic pressure on membrane permeability. In order to simulate measurement conditions in the field, a laboratory apparatus was constructed to control sample flow rate, temperature, pressure, and solution composition. The pressure correction methodology developed in this study was then applied to in situ underwater mass spectrometer data to generate high-resolution vertical profiles of dissolved gases in the Gulf of Mexico.

In situ measurements of sediment porewaters require analysis of very small sample volumes at very low flow conditions. Chapter 3 discusses the development of an automated sediment probe coupled with an underwater syringe pump that permits precise control of sample flow rate and intake location. To demonstrate this capability in the field, an underwater mass spectrometer was deployed on the Georgia continental shelf (depth = 27 m) to measure dissolved gas concentrations in the porewaters of highly permeable, medium-grained sands. Persistent porewater advection in these sands

considerably magnifies the ecological significance of benthic fluxes on Georgia's broad, shallow continental shelf (Jahnke et al., 2005).

Due to capabilities for measuring not only ambient levels of dissolved carbon dioxide, but also total dissolved inorganic carbon (DIC), MIMS instruments are well-suited for comprehensive carbon system determinations in seawater. Measurement of compatible carbon system parameters (e.g., DIC and either CO_2 concentration or fugacity) on a single platform allows comprehensive characterization of the marine CO_2 system. Chapter 4 explores characterization of MIMS carbon system measurements wherein an underwater mass spectrometer was used to investigate (a) relationships between sample flow rate and kinetic behavior at the MIMS membrane/solution interface (b) linearity of MIMS instrument response over a wide range of carbon dioxide concentrations, and (c) the influence of sample salinity on membrane permeability.

The ability to measure carbon dioxide partial pressure, DIC and other important marine analytes (e.g. methane, dinitrogen, oxygen, argon, hydrogen sulfide, total sulfide, and dimethylsulfide) in a wide range of oceanic environments establishes underwater MIMS as a uniquely capable means of characterizing both aerobic and anaerobic ecosystems in situ.

Chapter 2: Calibration of an In Situ Membrane Inlet Mass Spectrometer for Measurements of Dissolved Gases and Volatile Organics in Seawater

Abstract

Use of membrane inlet mass spectrometers (MIMS) for quantitative measurements of dissolved gases and volatile organics over a wide range of ocean depths requires characterization of the influence of hydrostatic pressure on the permeability of MIMS inlet systems. In order to simulate measurement conditions in the field, a laboratory apparatus was constructed for control of sample flow rate, temperature, pressure, and the concentrations of a variety of dissolved gases and volatile organic compounds. MIMS data generated with this apparatus demonstrated that the permeability of polydimethylsiloxane (PDMS) membranes is strongly dependent on hydrostatic pressure. For the range of pressures encountered between the surface and 2000 m ocean depths, the pressure-dependent behavior of PDMS membranes could not be satisfactorily described using previously published theoretical models of membrane behavior. The observed influence of hydrostatic pressure on signal intensity could, nonetheless, be quantitatively modeled using a relatively simple semi-empirical relationship between permeability and hydrostatic pressure. The semi-empirical MIMS calibration developed in this study was applied to in situ underwater mass spectrometer (UMS) data to generate high-resolution vertical profiles of dissolved gases in the Gulf of Mexico. These measurements constitute the first quantitative observations of dissolved gas profiles in the oceans obtained by in situ membrane inlet mass spectrometry.

Alternative techniques used to produce dissolved gas profiles were in good accord with UMS measurements.

Introduction

Since the late 1990's underwater mass spectrometer (UMS) systems have been under development for direct measurements in freshwater and seawater (Gereit et al., 1998; Short et al., 1999; Hemond and Camilli, 2002). Many field portable mass spectrometers, including submersible systems, depend on the use of membrane inlets (Kotiaho, 1996; Matz et al., 1999; Johnson et al., 2000; Bossuyt and McMurtry, 2004; Camilli and Hemond, 2004; Tortell, 2005; Short et al., 2006; Janfelt et al., 2006). Membrane inlets are advantageous as a means of reducing sample preparation requirements and decreasing gas loads on vacuum pumps. In addition, membrane inlets are rugged and allow many simple gases and volatile organic compounds (VOCs) to be monitored simultaneously (Thompson et al., 2006).

Membrane inlet mass spectrometry (MIMS) has been used for chemical measurements since 1963 (Hoch and Kok, 1963). However, many of the complexities of membrane inlet systems are still under investigation (Futo and Degn, 1994; Ørsnes et al., 1997; Hansen et al., 1996), and theoretical treatments of gas permeation in polymers have been met with varying degrees of success (Klopffer and Flaconneche, 2001; Lipnizki and Trägårdh, 2001). Although Fick's Law describes a simple linear relationship between analyte flux and partial pressure or fugacity gradient, permeation characteristics can change when a polymer membrane undergoes compression, swelling, competitive sorption, or changes in geometry (Fujita, 1961). Some of these potential complexities are not relevant to environmental measurements. For example, significant swelling and

competitive sorption are not expected with aqueous samples (Favre et al., 1994), and properly supported membranes greatly reduce the potential significance of changes in system geometry under pressure. For aqueous samples, the principal expected influences on the behavior of membrane inlet systems are temperature, pressure and hydrodynamics at the MIMS membrane/solution interface.

Calibration of membrane permeability as a function of temperature, pressure and system hydrodynamics is likely to be a formidable task. In view of this expectation, it has proven advantageous to perform in situ MIMS measurements at constant temperature and flow conditions (LaPack et al., 1990). The MIMS systems described in this work provide continuous sample-flow at constant temperature, whereupon variable hydrostatic pressure is the predominant uncontrolled influence on the membrane inlet system. Although control of hydrostatic pressure in MIMS systems is inherently feasible, such a capability is likely to substantially reduce sample throughput and add undesirable complexity to MIMS measurements. Therefore, in order to extend the capabilities of MIMS systems to observe important phenomena in the deep sea (e.g., hydrothermal venting and benthic fluxes, including those emanating from methane hydrates), the performance of MIMS inlet systems must be characterized over a wide range of pressure.

Herein we report the effect of hydrostatic pressure on the permeability of a polydimethylsiloxane (PDMS) membrane to dissolved gases and VOCs. Physical mechanisms for hydrostatically-induced variations in membrane permeability are discussed, and a semi-empirical equation is developed to describe the dependence of membrane permeability on hydrostatic pressure. Our characterization of PDMS membrane behavior is used to quantitatively interpret in situ MIMS observations of

dissolved gases in the Gulf of Mexico. The performance of the MIMS system is then evaluated through comparisons with measurements obtained using conventional oceanographic methods.

Theory

Steady State Permeation. The permeability (P_G) of gas G through a membrane can be described in terms of a solution-diffusion mechanism (LaPack et al., 1990):

$$P_G = D_G K_G \quad , \quad 2.1$$

where D_G is the diffusion coefficient of gas G in the membrane, and K_G is a gas partition coefficient defined as the quotient of the dissolved gas concentrations on the membrane side and the solution side of the membrane-water interface. Fick's First Law defines the gas flux (F_G) in steady state at location (x) in the membrane:

$$F_G = -P_G A \left(\frac{dC_G(x)}{dx}\right) = -D_G K_G A \left(\frac{dC_G(x)}{dx}\right) \quad , \quad 2.2$$

where A is the membrane area, and $dC_G(x)/dx$ is the gas concentration gradient at x. Mass spectrometer ion current intensity is proportional to gas flux through the membrane and, for our case, can be related to sample dissolved gas concentrations via the solution to Fick's First Law for a cylindrical flow-over membrane:

$$F_G(r_i) = \frac{2\pi L D_G K_G (C_{G,o} - C_{G,i})}{\ln\left(\frac{r_o}{r_i}\right)} \quad , \quad 2.3$$

where L is the membrane length, and ($C_{G,o}$ -$C_{G,i}$) is the difference in gas concentrations between the cylindrical membrane's outer (r_o) and inner radius (r_i). In the case that a vacuum is maintained within the membrane capillary, $C_{G,1}$ is negligible compared to $C_{G,2}$.

Laminar flow at the surface of the membrane intensifies analyte depletion at the membrane surface and reduces the steady-state analyte flux (Sysoev, 2000; Woldring, 1970). Analyte depletion in the boundary layer can be partially mitigated by a high sample flow rate through restrictive geometries around the membrane. As the depletions are dependent upon sample velocity, a constant flow rate is required to obtain quantitative results.

Non Steady-State Permeation. Characterization of non steady-state membrane permeation can be gained through analysis of step function dynamics. For cylindrical membrane *ro/ri* values less than about four, the theoretical solution for a stepwise increase in sample concentration is closely approximated by that of a sheet membrane (Pasternak et al., 1970; Crank, 1975):

$$F_{G,t} = F_{G,ss}\left(1 + 2\sum(-1)^n e^{\left(\frac{-n^2\pi^2 D_G t}{l^2}\right)}\right) \quad , \qquad 2.4$$

where l is membrane thickness, $F_{G,\,t}$ is gas flux at time, t, and $F_{G,\,ss}$ is gas flux at steady-state. Diffusion coefficients can be determined by fitting eq 2.4 to a concentration step function. Accurate descriptions are obtained using only a few terms in the summation.

Molar Volume Correction. Pressure influences the activities of permeants in both the solution and the membrane. Changes in partition coefficients with pressure can be described in terms of the difference between the molar volumes of a given permeant in different solution phases (Wijmans, 2004). As such, partition coefficient variations with pressure are described as follows (Millero, 2005):

$$\frac{K_G^p}{K_G^0} = e^{\frac{-\Delta V_{G,m}(p-p^0)}{RT}} \quad , \qquad 2.5$$

where K_G^p is a partition coefficient at pressure p, K_G^0 is a partition coefficient at standard pressure, p^o (0.101 MPa), $\Delta V_{G,m}$ is the difference between a gas partial molar volume in the membrane and the liquid phase, R is the ideal gas constant (8.31 cm^3 MPa/mol K), and T is Kelvin temperature.

Experimental Methods

Membrane Characterization. The membrane inlet assembly used in this study was developed for underwater mass spectrometry at depths to at least 2000 m, where hydrostatic pressure is approximately 20 MPa. Although this was the maximum pressure used for the tests performed here, we have observed that the membrane can support pressures of at least 40 MPa.

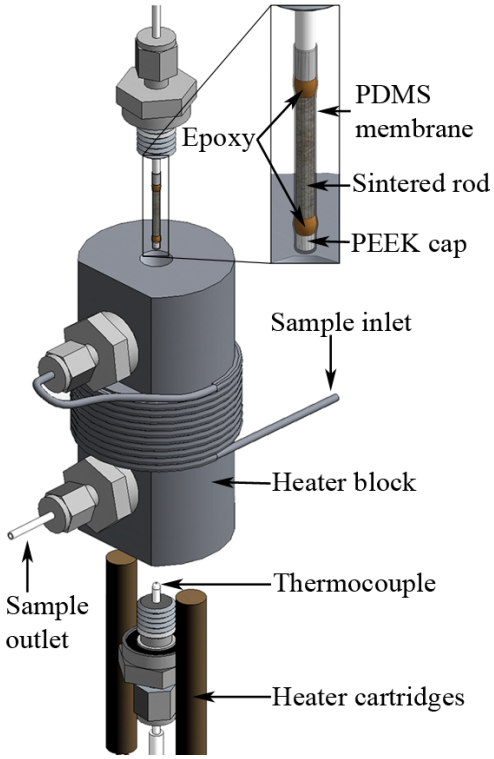

Figure 1. A view of the high pressure flow over membrane inlet assembly. Before sample enters the heater block, several wraps of the sample tubing around the block warm the sample solution. The heater cartridges regulate temperature adjacent to the membrane at the center of the heater block. Restrictive dimensions around the membrane produced high sample flow velocities (~15 cm/s) using moderate flow rates (~8 mL/min) while allowing passage of particulates.

The membrane inlet assembly, Figure 1, consisted of a hollow fiber PDMS membrane (0.064 cm *i.d.*, 0.119 cm *o.d.*) (Model 60-011-03; Helixmark, Carpinteria, CA, USA) mounted in a stretched state on a porous sintered Hastelloy C rod (0.14 cm *o.d.* 0.75 cm length, 2 μm pore size). The supported membrane was capped on one end with a 2 mm length of polyetheretherketone (PEEK) rod (0.14 cm *o.d.*) and epoxy, while the other end was connected using epoxy and a Swagelok fitting to the vacuum chamber via a 10 cm length of stainless steel tubing (0.127 cm *i.d.*, 0.159 cm *o.d.*). The membrane assembly was inserted into a stainless steel heater block (0.25 cm *i.d.*, 3 cm *o.d.*) that also housed a thermocouple and heater cartridges for controlling sample and membrane

temperature (+/- 0.1 °C of the set point). During variable flow experiments, a secondary heater was used to pre-heat samples to the set point before entry into the membrane assembly. This significantly reduced temperature fluctuations at the membrane.

The membrane inlet assembly was fitted to a Transpector 2.0 quadrupole residual gas analyzer (Inficon, Syracuse, New York) installed in a custom vacuum housing that was regulated at 100 °C. The chamber was evacuated using a turbo-molecular pump (Model V70LP; Varian, Palo Alto, CA, USA) backed by a dry diaphragm roughing pump (KNF Neuberger, Inc, Trenton, NJ, USA). Open source electron impact ionization was performed with a thoriated tungsten filament. An electron multiplier was used for detection of ions. Samples were passed through the membrane inlet assembly at 8 mL/min using a high performance liquid chromatography (HPLC) pump (Shimadzu, Kyoto, Japan). Hydrostatic pressure at the membrane was monitored with a digital pressure gauge (Cecomp Electronics, Libertyville, IL, USA) fitted to the sample outlet. Pressure was controlled manually using a backpressure regulator (Swagelok, Solon, OH, USA). A schematic of the experimental setup is shown in Figure 2. A pulse dampener (Restek, Bellefonte, PA, USA) reduced pressure pulses to less than 1% of the ambient pressure. Sample flow rate was periodically measured manually to ensure that flow rates were consistent with flows defined by the HPLC pump. The maximum sample pressure was limited to 20 MPa by the HPLC pump. A stream selection valve (VICI Valco Instruments, Houston, TX, USA) was used to control the sample introduction and to provide user-defined proportional mixing of samples in order to obtain calibration curves.

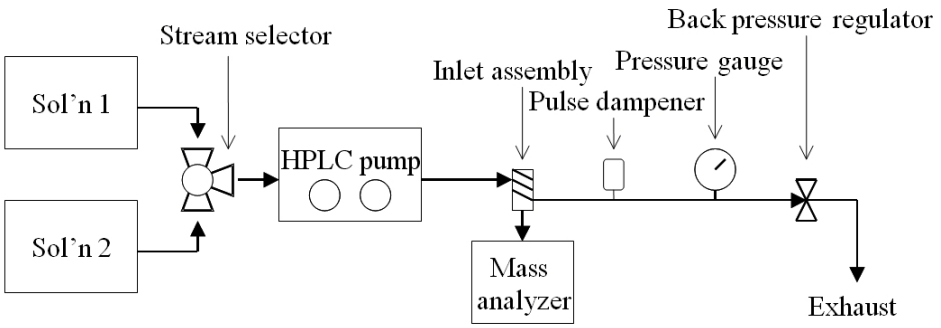

Figure 2. Lab apparatus for membrane inlet experiments. Sample concentration, flow rate, temperature, and pressure at the membrane inlet can each be controlled independently. Sample concentrations were determined by mixing two or more solutions at selected ratios by switching the valve at specified duty cycles at high frequencies. Linear concentration calibration plots can be obtained for a wide range of hydrostatic pressure set-points.

The primary calibration solution containing simple dissolved gases was prepared by sparging (>1 hr) phosphate-buffered deionized water (pH = 3.7, T = 25°C) with a calibrated gas mixture (Airgas, Radnor, PA, USA) containing 21% oxygen, 0.9% argon, 0.1% carbon dioxide, 0.1% methane, and nitrogen as the balance gas. The low pH of the phosphate-buffered solution reduced the sum concentration of HCO_3^- plus CO_3^{2-} to less than 0.3% of the total dissolved CO_2 concentration. Dissolved gas concentrations were determined using MATLAB (Version R2006a; Mathworks, Natwick, MA, USA) scripts developed from a variety of sources (Weiss, 1974; Hamme and Emerson, 2004; Wiesenburg and Guinasso, 1979; Garcia and Gordon, 1992). A second solution, deionized water at a vigorous boil (>1 hr), served as a blank. A constant temperature bath (25 °C) cooled the water inline, upstream of the stream selector valve.

A third solution containing dissolved VOCs was prepared by adding small quantities of dimethyl sulfide, benzene, chloroform, and toluene to 10mL of methanol. An aliquot of the methanol solution (1.5 mL) was then added to 1 L of deionized water in

a septum-sealed flask. Subsequently, sodium sulfide nonahydrate (0.2 g) and 1,4-dioxane (0.56 mL) were directly added to the 1 L solution, and monobasic potassium phosphate was used to buffer the pH to 5.3. All chemicals were obtained from Sigma-Aldrich, St. Louis, MO, USA. Concentrations were chosen to create signal intensities that, at minimum, were an order of magnitude above the baseline values for each ion. The requisite concentrations for VOC analyses were determined by incremental additions of each VOC to an experimental solution. It was noted that, upon addition of each VOC, the ion currents for other VOCs did not change. This indicates that the *m/z* values chosen for quantification of each analyte (Table 1) were free of interferences, and that there was no detectable swelling of the membrane as a result of VOC sorption.

Table 1. Ions and permeant concentration used for analysis of permeability.

Analyte	mass/charge	Concentration (μmol/kg)
Methane	15	1.4
Water	17	55.6×10^6
Nitrogen	28	473
Methanol	30	37×10^3
Oxygen	32	251
Hydrogen sulfide	34	1.2×10^3
Argon	40	11.8
Carbon dioxide	44	34.1
Dimethyl sulfide	62	100
Benzene	78	9.9
Chloroform	83	10
1,4-Dioxane	88	6.6×10^3
Toluene	91	0.99

Relative changes in signal intensity were assumed to be proportional to relative changes in membrane permeability. With the exception of water, all signals were baseline subtracted. The baseline of water is known to be small relative to the signal intensity attributed to membrane permeation. Baseline values were determined by two independent methods that were in complete agreement: (1) sampling water that was being degassed by vigorous boiling; and (2) reducing of sample flow rate to zero, whereupon the aqueous sample in contact with the membrane became completely degassed. In the

latter case, degassing was exponential, with 90% degassing occurring in about 1.5 min (Figure 3). The latter method is particularly convenient as it also provides a simple and effective method for the determination of baseline values in the field. Furthermore, subsequent to sample degassing, diffusion coefficients can be determined by returning the pump to its set flow rate, whereupon a step-change in concentration occurs at the membrane surface. This procedure avoids the step function dispersion that would result during propagation of a concentration interface through a length of small diameter tubing. As mass spectrometer response times are much faster than membrane response times, the observed signal step function was used to determine diffusion coefficients via eq 2.4 and the non-linear fitting algorithms provided by MATLAB.

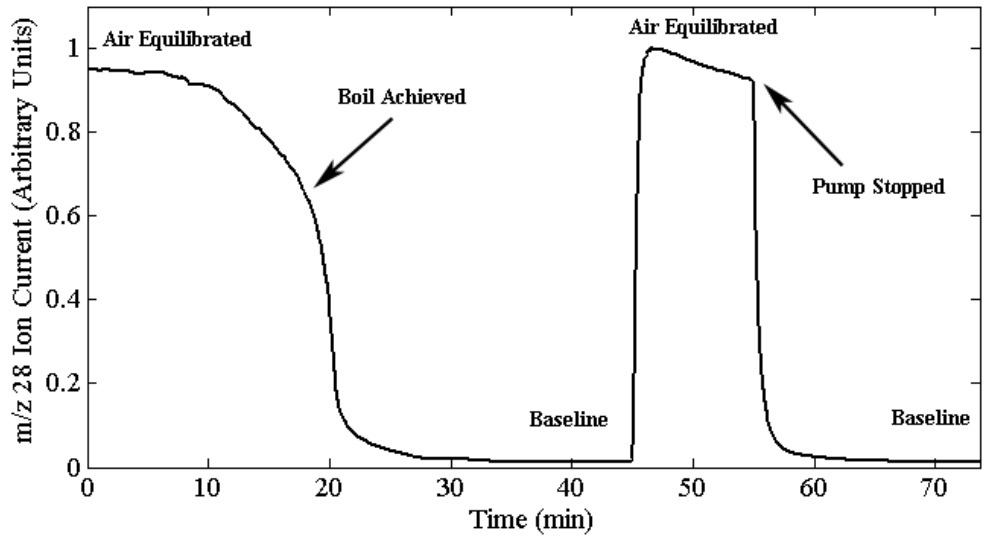

Figure 3. Demonstration of the two methods of blank preparation. 1) Air equilibrated deionized water was sampled while being brought to a vigorous boil. 2) Sample pump was stopped and the sample in contact with the membrane was completely degassed.

Boundary layer conditions have a strong influence on measurements of permeability and diffusion (Krogh et al., 2006), so it is meaningful to report these parameters only in a relative sense, normalized to ambient atmospheric pressure.

Furthermore, changes in membrane permeability due to changing hydrostatic pressure results in varying degrees of boundary layer depletion, making changes in signal intensity a summation of two influences. To address this point, experiments were performed using a range of flow rates. For the membrane inlet configuration used in the present study, variations in boundary layer depletion that resulted from changes in membrane permeability were negligible at flow rates above ~6 mL/min. Thus, changes in signal intensity with hydrostatic pressure were effectively only a function of changing membrane permeability. This observation is demonstrated in Figure 4 by the ratio of signal intensity at ambient pressure to signal intensity at 10 MPa, which becomes independent of the flow rate at elevated rates.

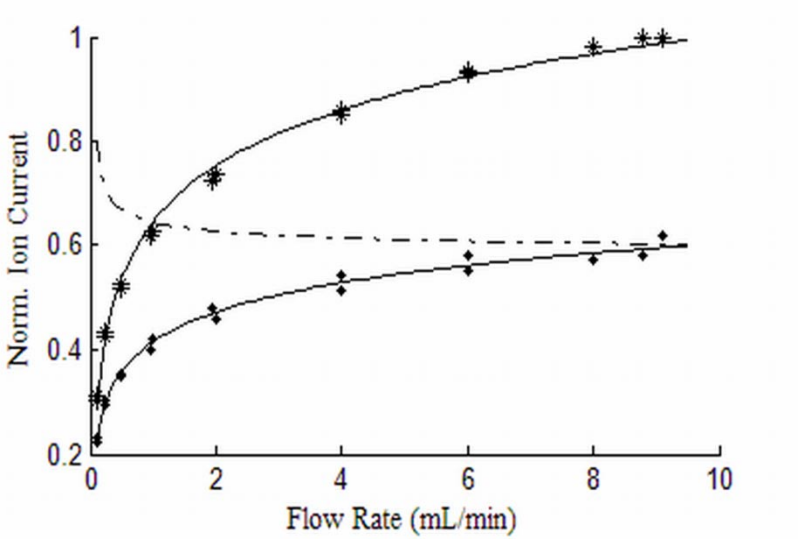

Figure 4. Ion current for *m/z* 28 (Nitrogen) at various flow rates. Data were collected at ambient pressures (*) and 10 MPa (♦) and each were normalized to flow at 9 mL/min. The dashed line represents the ratio of data at ambient pressure and 10 MPa. A decrease in membrane permeability results in a decrease in the boundary layer thickness. Thus, the ratio increases at low flow rates. At higher flow rates, the boundary layer is small and the decrease in boundary layer thickness will be insignificant compared to the change in membrane permeability. Thus, changes in ion current are a result of changes in membrane permeability.

Field Experiment. UMS field measurements were obtained using previously described instrumentation (Short et al., 2001) with the following modifications: the membrane assembly was replaced with the high pressure assembly described above; the sample pump was replaced with a custom-made system capable of generating 10 mL/min flow rates at 42 MPa, with a power requirement near 1 W, and the tungsten filament was replaced with an yttria-coated iridium filament. The Ir/Y_2O_3 filament has a lower work function than tungsten and, being inert relative to tungsten, provides longer lifetimes at elevated water and oxygen partial pressures (Harvey, 1974). This reduces gas-filament reactions that have been shown to create high baselines (Hoch and Kok, 1963; Ørsnes et al., 1997) and other problems (Kana et al., 2004).

Field data were collected on the West Florida Shelf in the Gulf of Mexico (27° 17.8' N, 85° 07.9' W) on August 8 and 9, 2006 using the Florida Institute of Oceanography's R/V Suncoaster. The UMS was mounted on an aluminum Rosette frame (General Oceanics Inc, Miami, FL, USA) with a custom-made battery pack, and an SBE 25 Sealogger conductivity, temperature and depth sensor (CTD) (Sea-Bird Electronics, Inc, Bellevue, WA, USA) (Figure 5). The CTD also accommodated a dissolved oxygen sensor (SBE 23). The package was deployed using a standard University National Oceanographic Laboratory System (UNOLS) oceanographic cable and winch. The battery stack consisted of 80 1.2 V 'C' sized nickel metal hydride batteries. The batteries were wired to produce 24 V, which allowed continuous UMS operation for more than 8 hours.

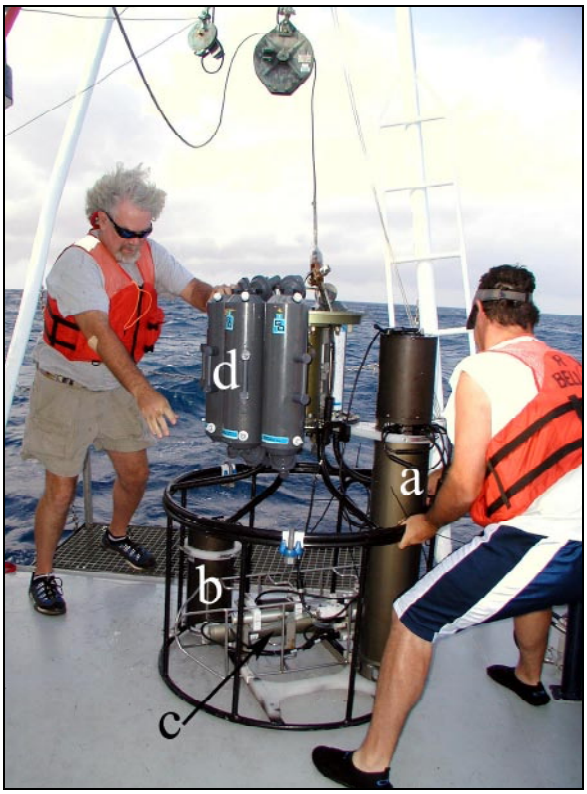

Figure 5. Deployment of the General Oceanic Rosette frame. On board were the following: a) UMS system b) batteries c) CTD d) Niskin water samplers.

An Ethernet extender (Patton Electronics, Gaithersburg, MD, USA) established high bandwidth real-time communications through the UNOLS cable. Although communication through the tether was intermittent due to a faulty winch slip ring, all data were recorded autonomously using the UMS embedded computer and Labview software (National Instruments, Austin, TX, USA) so data collection was not affected. The UMS computer also recorded depth, temperature, salinity, and dissolved oxygen from the CTD. Temperature and salinity data were used for calculation of seawater gas saturation states (Hamme and Emerson, 2002) relative to equilibrium with the atmosphere.

UMS deployment parameters were as follows: selected ion scan mode; 256 ms dwell time for *m/z* 14, 28, 32, 34, 40, 44, 62 and 64 ms dwell time for *m/z* 2, 12, 15, 16,

17, 18, 20, 29, 30, 36, 45, 47, 67, 73, 78, 91 yielding a 3.5 s scan time per cycle; 1000 V electron multiplier; 40 eV electron energy; 200 mA electron current; 4 mL/min sample flow rate; and 35 °C membrane temperature. Prior to deployment, a three-point instrumental calibration was performed for methane, nitrogen, oxygen, argon, and carbon dioxide. Intercept (zero) concentrations were created at zero sample flow whereby surface seawater made stationary in contact with the membrane was completely degassed. Two additional calibration solutions were generated by sparging surface seawater (S = 36.5, T = 25.5 °C) for more than 30 minutes with calibrated gas standards (Airgas, Radnor, PA, USA).

Three UMS casts were performed over two days. These casts were to a depth of 500 m, about 20 m short of the seafloor. During the first cast, the UMS sampled the water column on both the downcast and the upcast. On the subsequent cast nine hours later the UMS sampled a 1 L Tedlar bag (SKC Inc, Eighty Four, PA, USA) that contained surface seawater equilibrated with a standard gas mixture. A third cast was performed the following day without the UMS. This cast was performed to examine the temperature and salinity profile of the water column. These data were absent from the first two casts due to a faulty CTD power supply. Table 2 outlines the sequence of events for each cast.

Table 2. Sequence of events for deployment of the UMS in the Gulf of Mexico.

Step	Activity	Depth (m)	Descent/Ascent Rate (m/min)	Duration (min)
1	Descent	0 to 30	20	1.5
2	Hold for bubble dissolution	30m	0	10
3	Return to surface	30 to 1	20	1.5
4	Descent to bottom	1 to 500	15	33
5	Hold for equilibration	500	0	5
6	Ascent to surface	500 to 1	15	33
7	Hold for Equilibration	1	0	1
8	Return to deck	n.a.	n.a.	<1

Results and Discussion

Membrane Characterization. MIMS ion currents were linearly dependent on concentration at both ambient and elevated hydrostatic pressures (data not shown). However, Figure 6 shows non-linear results for MIMS ion currents plotted against hydrostatic pressure for a selection of dissolved gases and VOCs. In the case of simple gases, ion current decreases with increased pressure, indicating a decrease in membrane permeability. Larger and non-polar permeants show an initial decrease in ion current, but an increase at higher pressure. The signal variations shown in Figure 6 are attributable to variations in membrane permeability that result from variations in diffusion coefficients

and/or partition coefficients. Figure 7 shows both components of permeability are pressure dependent.

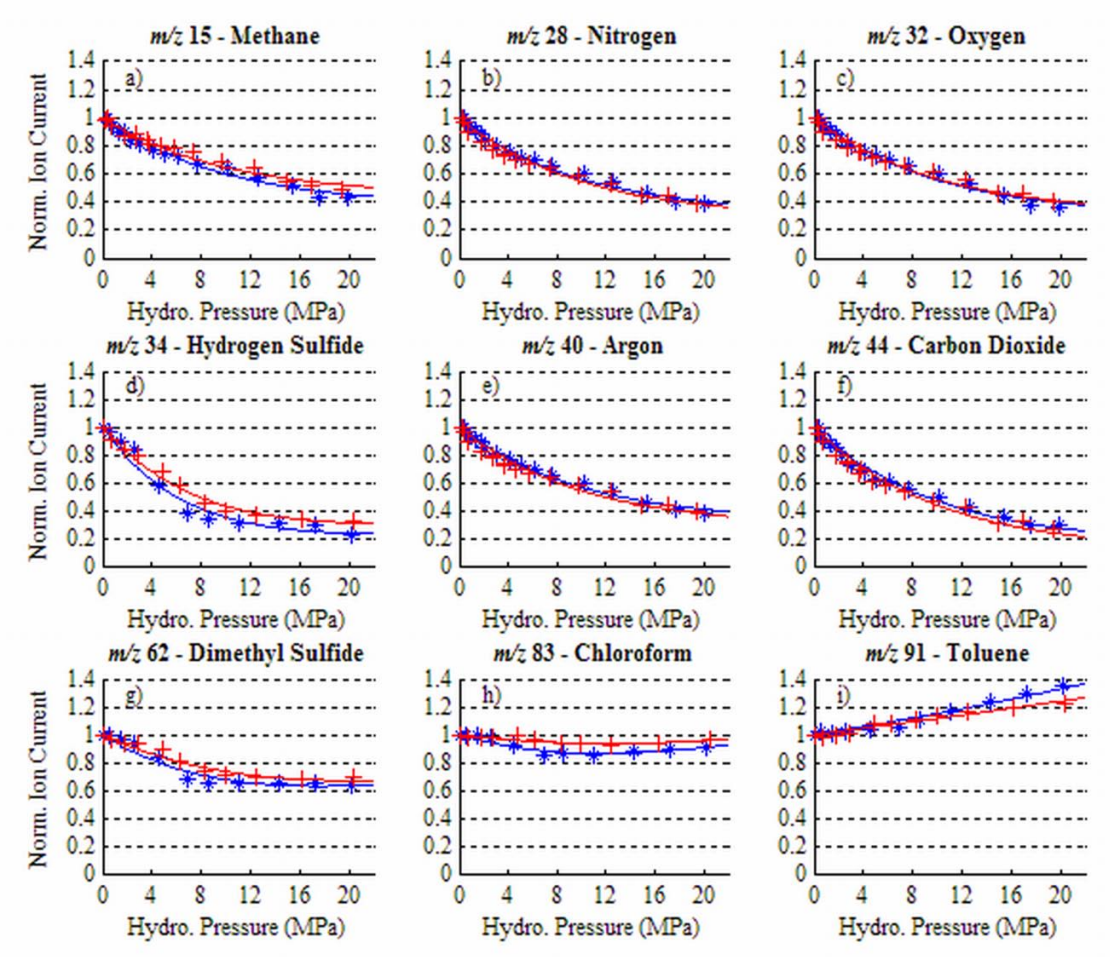

Figure 6. Ion current dependency on hydrostatic pressure for selected permeants. Blue (∗) data were obtained as hydrostatic pressure was increased, and red (+) data as pressure was decreased. Data were normalized to the ion current at 0.1 MPa (ambient), and fitted using eq 2.7. Data shown were obtained at 35 °C.

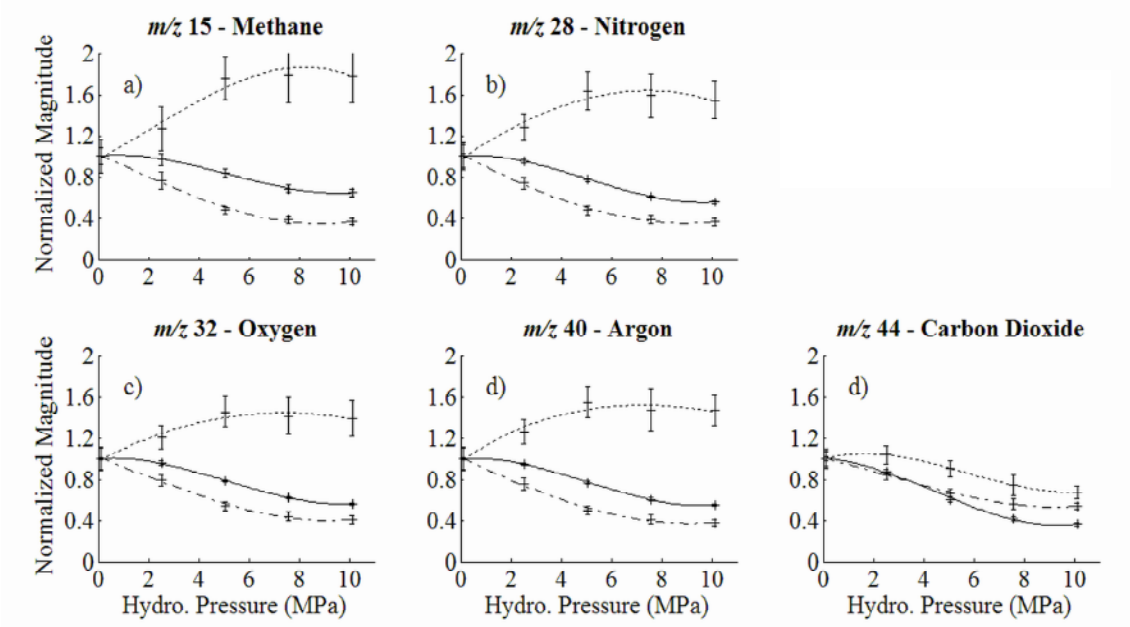

Figure 7. Change in membrane transport behavior with hydrostatic pressure. Permeability (---), diffusion (-··-), and partition coefficients (···) data are determined at 35 °C, are normalized to 0.1 MPa, and fit with polynomial to visually link the data. Relative permeability coefficients were determined using steady state signal intensity, relative diffusion coefficients were extracted from concentration step functions and relative partition coefficient were calculated via eq 2.1.

Toward the goal of simple quantitative membrane inlet calibrations with respect to pressure, several models were applied to the permeability data embodied in Figure 6. However, the utility of each model was limited by (a) the large number of coefficients required to obtain acceptable data-fits and (b) unrealistic extrapolations that were obtained using the best-fit coefficients of each model. Consequently, the pressure dependence of membrane permeability for small permeants was assessed using the following simple, semi-empirical model:

$$\frac{P^p}{P^0} = k + (1-k)e^{-b'p} \quad , \qquad 2.6$$

where *k* corresponds to the fraction of an analyte's permeability that is independent of pressure, and *b'* is related to polymeric free volume and, therefore, membrane compressibility. For a given membrane, best-fit *b'* values are approximately constant for different permeants, while *k* values are specific to each permeant. For small polar compounds, *k* values are small, suggesting a strong permeation dependence on polymeric free volume. Large non-polar compounds have *k* values near 1, indicating a minimal dependence on polymeric free volume, and a propensity for dissolution within the structure of the polymer.

Equation 1.6 does not predict the increase in ion current observed for many VOCs. For large permeants, a molar volume term can be included. This is achieved by combining the concepts developed in eqs 2.5 and 2.6 to produce the following semi-empirical expression:

$$\frac{P^p}{P^0} = \left(k + (1-k)e^{-b'p}\right)e^{\frac{-\Delta V_{G,m}\left(p-p^0\right)}{RT}} \qquad 2.7$$

Significant differences are expected in the molar volumes of large non-polar molecules within a polar solvent (water) and the non-polar polymer (PDMS). Positive increases in permeability with pressure indicate that the molar volumes of large non-polar permeants in PDMS are smaller than in water. Equation 2.72.72.7 coefficients for 13 permeants were determined via non-linear fits at 35 °C and 15 °C as pressure was increased (simulating downcast condition) and as pressure was decreased (simulating upcast conditions). The coefficients reported in Table 3 varied with temperature and membrane history, and were specific to individual membrane inlets. Notably, the

temperature-dependent *k* values indicate that MIMS system pressure calibrations are greatly simplified by maintaining constant membrane temperature. Values for $\Delta V_{G,m}$ have the correct order of magnitude relative to those reported by Kamiya et al. (Kamiya et al., 2000). Also, Table 3 shows that hysteresis in the MIMS response produces significant uncertainties in $\Delta V_{G,m}$ determinations. Hysteresis can be attributed to imperfect PDMS elasticity, and is consistent with compression characteristics reported in the product datasheet. Increased precision for $\Delta V_{G,m}$ and slightly better fits are achieved if *b'* is allowed to vary between analytes.

Table 3. Equation 1.7 coefficients for various permeants determined by non-linear least-square analysis. [1]

Analyte	k^2 (35 °C)		$k^{2,3}$ (15 °C)		$\Delta V_{G,m}{}^{2,4}$ (35 °C)	
	Downcast	***Upcast***	***Downcast***	***Upcast***	***Downcast***	***Upcast***
Methane	0.37 ± 0.04	0.44 ± 0.05	0.27 ± 0.05	0.25 ± 0.03	0^4	0^4
Water	0.35 ± 0.04	0.32 ± 0.05	-	-	0^4	0^4
Nitrogen	0.31 ± 0.03	0.33 ± 0.04	0.21 ± 0.02	0.23 ± 0.05	0^4	0^4
Methanol	0.47 ± 0.07	0.51 ± 0.05	-	-	0^4	0^4
Oxygen	0.29 ± 0.04	0.35 ± 0.04	0.23 ± 0.04	0.24 ± 0.04	0^4	0^4
Hydrogen sulfide	0.03 ± 0.1	0.13 ± 0.07	-	-	0^4	0^4
Argon	0.31 ± 0.03	0.32 ± 0.04	0.24 ± 0.03	0.26 ± 0.04	0^4	0^4
Carbon dioxide	0.18 ± 0.04	0.15 ± 0.04	0.08 ± 0.01	0.07 ± 0.04	0^4	0^4
Dimethyl sulfide	0.52 ± 0.06	0.59 ± 0.04	-	-	0^4	0^4
Benzene	0.6 ± 0.1	0.93 ± 0.09	-	-	52 ± 21	16 ± 11
Chloroform	0.5 ± 0.2	0.8 ± 0.1	-	-	53 ± 46	19 ± 20
1,4-Dioxane	0.5 ± 0.3	0.7 ± 0.2	-	-	85 ± 60	46 ± 29
Toluene	0.8 ± 0.1	1.1 ± 0.1	-	-	57 ± 17	20 ± 15

(1) Downcast data were normalized to data obtained prior to pressurization and upcast data were normalized to data obtained after depressurization.
(2) *b'* was determined as 0.10 ± 0.03 MPa^{-1} at 35 °C and 0.13 ± 0.07 MPa^{-1} at 15 °C. Although use of *b'* as a best-fit variable between gases and casts would improve estimates of *k* and $\Delta V_{G,m}$. This provides only small improvements in calibrations.
(3) VOCs and water were not analyzed at 15 °C.
(4) Values reported as zero for $\Delta V_{G,m}$ were set to zero as there was no indication that signal intensity increased with pressure, which reduced the number of calibration coefficients without a loss in accuracy for this pressure range.

Field Data. Several UMS dissolved gas profiles obtained in the Gulf of Mexico are presented in Figure 8. VOC depth profiles were, as expected in the open ocean, below instrument detection limits. Figure 8a-c show UMS signals at *m/z* 17 (water), *m/z* 28 (nitrogen) and *m/z* 32 (oxygen) expressed in terms of concentrations via calibrations at one atmosphere hydrostatic pressure. Water activity is dependent on temperature and, to a lesser extent, salinity (Millero and Leung, 1976). Since the membrane temperature was

35 °C and salinity was essentially constant between the surface and 500 m, the water profile shows a decrease with depth that must be attributable to compression of the PDMS membrane. Nitrogen and oxygen profiles differ distinctly from the water profile. Nitrogen concentrations in seawater are strongly dominated by ambient seawater temperature and salinity during equilibration with the atmosphere. Since neither temperature nor nitrogen concentrations are substantially altered during water mass subduction, the nitrogen profile shown in Figure 8b increases with depth in response to decreasing in situ temperature. Oxygen concentrations are influenced strongly by both physical and biological processes. Subsequent to atmospheric equilibrium, dissolved oxygen concentrations are, like nitrogen, inversely related to both temperature and salinity. Photosynthesis at shallow depths typically produces small supersaturations with respect to atmospheric equilibrium, and net respiration at greater depths typically reduces oxygen concentrations to levels much below saturation. All of these influences are seen in Figure 8c.

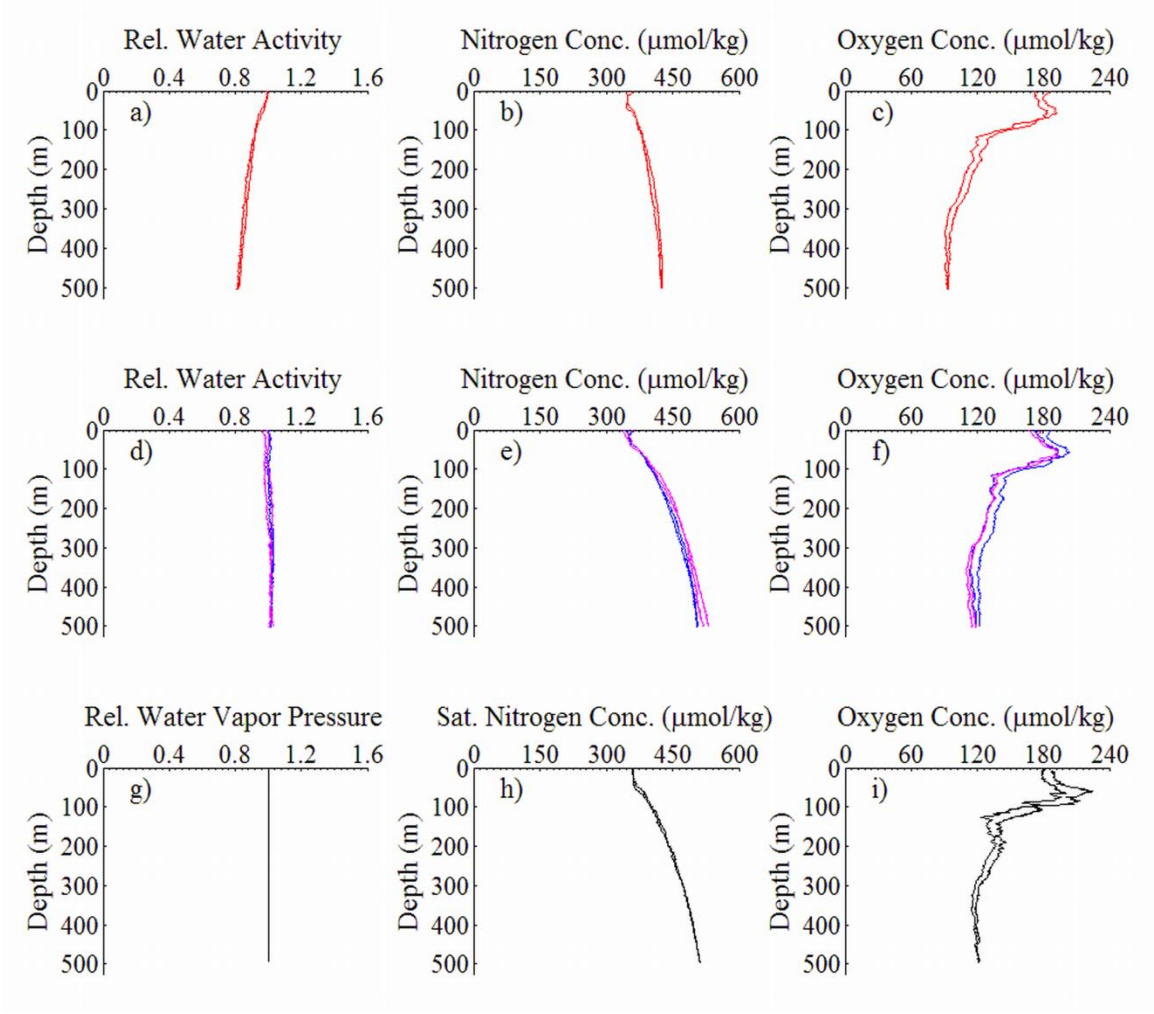

Figure 8. Concentration depth profiles from the Gulf of Mexico. Figures a, b, and c were obtained using 0.1 MPa concentration calibrations. Figures d, e, and f show pressure corrected data; the blue lines were corrected using eq 7, and the magenta lines were corrected using data obtained with a standard solution. Figures g, h, and i show data determined with an independently-deployed CTD and oxygen sensor. Downcasts and upcasts are shown.

Although the influence of membrane compression on signal intensities is seen most clearly in Figure 8a, it is apparent that membrane compression is an important effect for all UMS observations. Two independent methods were used to account for the effects of hydrostatic pressure on instrument response. In the first case, calibration coefficients obtained via eq 2.6 were used to generate the activity and concentration profiles (blue) shown in Figure 8d-f. Although this method is complicated by calibration coefficients

that may vary between casts, it provides an essential first order account of pressure-corrected instrument response when deployment logistics do not allow in situ calibration, as described below.

As an alternative to pressure corrections via eq 2.6, the pressure dependence of UMS signals was examined while the UMS sampled a standard solution during a follow-up profile to 500 m. The data from this follow-up profile were normalized to the UMS signal intensities obtained while the standard solution was sampled at the surface. High frequency noise was smoothed using a 4^{th} degree polynomial fit. These data were then used to correct the raw in situ data obtained during the first cast. The results obtained in this analysis, which provide a first order account of the influence of membrane deformation kinetics on UMS measurements, are shown in Figure 8d-f (magenta, downcast and upcast). The juxtaposition of magenta and blue profiles shows no systematic depth-dependent differences between calibration methods. It appears then that hysteresis is a minor influence in the upper 500 m and can be accounted for quantitatively. Nevertheless, it should be noted that this type of procedure should become increasingly important if UMS observations were to include a wider range of depth in the water column.

Figure 8g-i show activity and concentration profiles that were determined independent of UMS observations. Water vapor pressure, calculated from salinity (Hamme, 2006) and normalized to vapor pressure at the sea surface, is shown vs. depth in Figure 8g. As directly observed in Figure 8d, in the absence of strong salinity gradients, variations in water activity (and hence vapor pressure) are expected to be very small. Figure 8h shows predicted nitrogen saturation concentrations (calculated from

temperature and salinity) for equilibrium with the atmosphere. Good accord is observed with the UMS data shown in Figure 8e and 8h. Figure 8i shows a dissolved oxygen profile obtained with the SBE 23 dissolved oxygen sensor. The data shown in Figure 8f and 8i are in close agreement and it can be noted that, due to hysteresis effects, the dissolved oxygen sensor shows downcast/upcast differences that are generally as large as or larger than those obtained by the UMS. These measurements, which constitute the first quantitative observations of dissolved gas profiles in the oceans obtained by in situ membrane inlet mass spectrometry, indicate that UMS systems are capable of providing unique quantitative assessments of fine-scale processes in the marine environment.

Chapter 3: Dissolved Gas Analysis of South Atlantic Bight Sediment Porewater by Flow-Through Membrane Introduction Mass Spectrometry

Abstract

An underwater membrane introduction mass spectrometer was deployed on the Georgia continental shelf (depth = 27 m) to measure in situ dissolved gas concentrations in sediment porewaters. Over a 54-hour period, 30 profiles of sediment porewater (up to 18 cm deep) were sampled using an automated sediment probe coupled with an underwater positive displacement syringe pump. The porewater was analyzed with a flow-through membrane assembly at constant sample flow rate (0.35 ml/min) and membrane temperature (45 °C). Calibration was performed using on-site seawater equilibrated with gas standards. During the seafloor deployment, spar buoys provided continuous power to the instrumentation as well as communication, allowing real-time data analysis and instrumental control.

Sediment at the deployment site is highly permeable medium to coarse grained sand. It is non-accumulating and has very low organic matter content. Measurements of methane, nitrogen, argon, oxygen and carbon dioxide concentrations were used to produce depth-time contours and demonstrate the dynamics of dissolved gases in the porewater. Porewater methane concentrations indicated the presence of methanogenic bacteria, and elevated methane concentrations in ambient water suggest that methane production in the sediment porewater may be a significant source of methane in the water ecosystem. Dynamic, elevated nitrogen-argon ratios suggest a complex denitrification-

nitrification system. Oxygen and carbon dioxide sediment profiles were closely coupled. A correlation between chemocline depth and sediment ripple height suggested that the porewater environment is controlled by water inundation and upwelling advection processes related to the presence of ripple troughs and crests respectively.

Introduction

Knowledge of dissolved gas concentrations in ecological porewaters is critical to understanding many complex environmental processes including nutrient cycling (Cornwell et al., 1999), climate change (Conrad, 1996), ground water contamination (Squillace et al., 1999), waste disposal (Sheppard et al., 2005), carbon sequestration (Ersland et al., 2009), and energy resource management (Reimers et al., 2006; Dickens et al., 1997; Lapham et al., 2008). However, porewater dissolved gas analyses present a particularly challenging set of logistical problems (Sansone et al., 2008). The dynamic nature of dissolved gases in natural systems demands sampling frequencies that are capable of resolving diurnal cycles and brief, episodic events. In some porewater systems, strong gradients necessitate sub-centimeter spatial resolution to accurately resolve the chemical profile (Benstead and Lloyd, 1994). Further, due to the volatility of gases, contamination of collected samples is a fundamental problem. This is particularly true for samples with fugacities that deviate significantly from fugacities in the atmosphere.

Some sampling problems can be mitigated by reproducing the natural environment of cored samples ex situ (Eyre et al., 2002; Kana et al., 1994). Extensive measurements of a core can then be obtained by non-destructive chemical analyses such as membrane inlet mass spectrometry (MIMS) (Kana et al., 1998), microelecrode potentiometry (Taillefert et al., 2000) or optrode (Klimant et al., 1995). Ideally, logistical considerations involving such procedures would include maintenance of temperature,

salinity, hydrostatic pressure, light intensity, fluid advection, and ambient water chemistry. As such, alternative in situ analytical options can be quite appealing.

MIMS has proven to be a reliable and multifaceted tool for analysis of dissolved gases in a wide variety of media, including sediment porewater (Lauritsen et al., 1992; Hansen and Degn, 1996; Johnson et al., 2000; An et al., 2001; Smith et al., 2008). Excellent spatial and temporal resolution has been achieved using MIMS probes, further they are capable of analyses of hydrogen, methane, dinitrogen, nitrous oxide, oxygen, hydrogen sulfide, argon, carbon dioxide and numerous volatile organic compounds (Tortell, 2005; Lauritsen and Gylling, 1995; Lloyd et al., 1996, 2002). Smaller and more efficient portable MIMS devices are increasingly used in the field to produce laboratory quality analyses, minimizing the likelihood of sampling artifacts (Lauritsen et al., 2008; Taylor and Bierbaum, 2008). It is natural then, that in situ analysis of sediment porewater by MIMS in the underwater environment be developed.

Previous MIMS analysis of sediment porewater analysis involved direct insertion of membrane probes into sediment cores ex situ. Though achieving excellent spatial resolution, such systems can control neither the probe's membrane temperature nor the probe's boundary depletion layer. In the present work, an underwater mass spectrometer (UMS) system with a flow-through membrane inlet assembly (Short et al., 1999) is used to examine sediment porewater in situ. As the flow-through inlet allows samples to be pumped to the MIMS, sample and membrane temperatures can be regulated thereby fixing membrane permeability. Further, by ensuring constant sample flow velocities at the UMS membrane interface during analysis, the flow-though inlet allows control of the boundary depletion layer at the membrane interface. Several problems are addressed by

achieving constant boundary layer conditions. (a) By flushing the boundary layer instrument sensitivity is maximized (Hartnett and Seitzinger, 2003); (b) changes in instrument response attributable to sediment tortuosity are averted (Sheppard and Lloyd, 2002); and (c) calibrations of carbon dioxide fugacity in solutions with a pH greater than 3 are enabled by fixing the contributions of HCO_3^-, and CO_3^{-2} to the carbon dioxide signal intensity. Perturbations in carbon dioxide fugacity are particularly intense and difficult to predict when the membrane boundary depletion layer is large and uncontrolled, as is the case with directly inserted membrane probes (Chapter 4).

Porewater analysis with a flow-through underwater mass spectrometer (UMS) system was conducted using a positive displacement syringe pump coupled to a vertically controlled sediment sampling probe. The UMS system was deployed for analysis on the Georgia continental shelf (depth = 27 m). Porewater and ambient water were sampled over a vertical distance of 18 cm. Integration of the sediment probe with the UMS's embedded computer enabled complex autonomous sampling protocols. This approach provides good sensitivity, obviates liquid nitrogen traps, mitigates analytical variables that influence signal intensity, and substantially simplifies system calibration. This work constitutes the first use of UMS for investigation of dissolved gases in sediment porewaters.

Study Setting and Methods

Sample Site. Data were collected (August, 2008) mid-shelf in the South Atlantic Bight (SAB) at the R2 Navy tower station (31° 22' N, 80° 34' W) (Figure 9). Work was conducted with the collaborative research program, Benthic Observatory and Technology Testbed On the Mid Shelf – Understanding Processes (BOTTOMS-UP). The R/V

Savannah was used to access the sample site and deploy instrumentation. Tidal height, wave height and light intensity data during the deployment were obtained from the R2 tower via the Skidaway Institute of Oceanography South Atlantic Bight Synoptic Offshore Observational Network (SABSOON) website (www.skio.peachnet.edu/Skioresearch/physical/sabsoon/). Sediments at the R2 site are non-accumulating, and have a 250-500 µm median grain size (Gorsline, 1963), high metabolic activity, low fine particulate content, and substantial benthic microalgal photosynthesis (Jahnke et al., 2005). Strong sediment-water interactions in this shallow continental shelf region, establishes the system's porewater chemistry as an essential component of the overall SAB ecosystem (Jahnke et al., 2005).

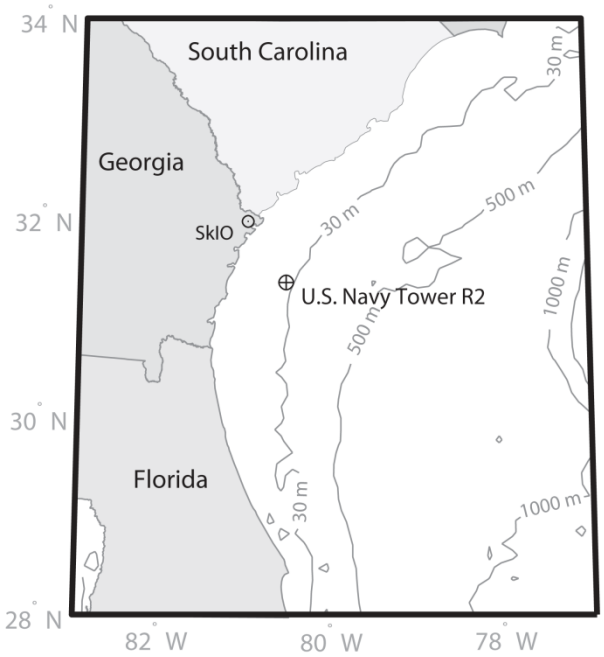

Figure 9. Deployment site located at US Navy Tower R2. The site is located 81 km offshore of Skidaway Institute of Oceanography (SkIO).

Sampling System. The sediment porewater sampling system was fabricated from an oil-filled vessel containing three stepper motors and a programmable controller board (Figure 10). The motors can be affixed to a variety of translational motion devices. For this study only two motors were operated. Motor 1 drove a lead screw fixed to a 5 mL sampling syringe to provide sample flow. Motor 2, also affixed to a lead screw, provided precise vertical control of a sediment sampling probe. Oil pressure in the vessel sustained at about 8 psi using a flexible polyurethane oil-water interface. This positive pressure ensures that seawater cannot enter the vessel in the event of a gasket or component failure. The total travel distance of the sediment probe (18 cm), was determined by the length of the lead screw.

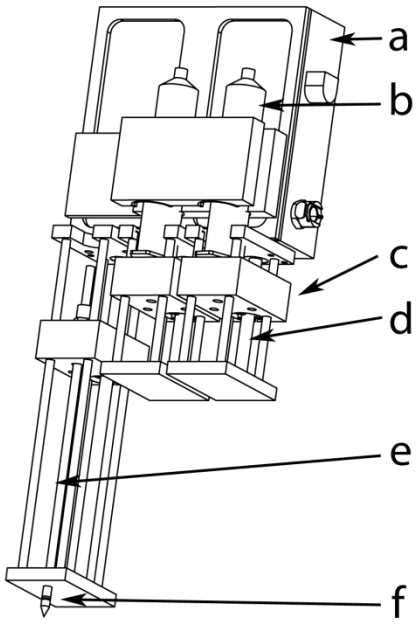

Figure 10. Sediment sampling sytem. a) oil filled vessel b) sampling syringes c) plunger d) lead screw e) sediment probe support tube f) sediment probe. Sampling tubes not shown for clarity.

The flow-through membrane inlet assembly and UMS system are similar to that previously published (Bell et al., 2007). A Hastelloy C (HC) sampling tube directly coupled the UMS membrane assembly inlet to the sediment probe tip. A second HC sampling tube coupled the membrane assembly outlet to the sampling syringe. A tee and two check valves fixed to the sampling syringe ensured that withdrawing the syringe plunger would cause porewater to travel from the sediment probe tip, through the membrane assembly, and into the syringe. When the syringe plunger was plunged, the check valves directed sample flow into the ambient seawater. Sample flow rate was set to 0.35 mL/min during analysis.

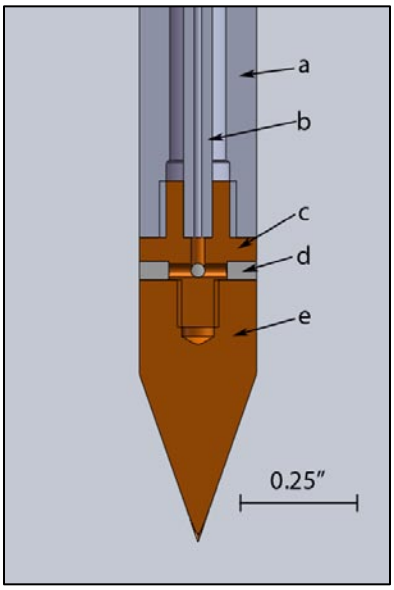

Figure 11. Sedimentary porewater sampling probe design. a) support tube b) sampling tube c) perforated base d) sintered intake filter e) penetrating tip.

The sampling probe consists of tip assembly, a 1.6 mm HC sampling tube, and a 6.4 mm stainless steel support tube (Figure 11). The tip assembly consists of an inlet filter sandwiched between a pointed polyaryletheretherketone (PEEK) tip and a perforated PEEK base. The base was threaded on both ends allowing construction of the

probe tip assembly. The perforated base directed porewater flow between the intake filter and sampling tube. A 6.4 mm diameter, 1.0 mm thick sintered HC disc with a 2 μm pore size and a 3.2 mm center-bore hole served as the intake filter. The sampling tube (0.76 mm i.d.) was press-fitted into the perforated base and epoxied in place to ensure a leak-free fit.

Deployment. The sampling system was mounted on a profiling frame that included an internally-logging conductivity-temperature-depth (CTD) sensor, a pressure vessel containing NiH batteries (which operated as a backup power source during power interruptions) and an underwater camera. The camera produced time-lapse photography of the sediment probe.

Two PVC spar buoys were tethered to the UMS system on the seafloor. The buoys contained sufficient Li-ion polymer batteries to allow 12 hours of UMS operation. As battery recharge time was less than 6 hours, replacement of the buoys every 12 hours allowed continuous UMS operation. To enable real-time UMS control and data monitoring, the tether routed DSL communications between the buoys and the UMS system. A wireless RF link was then used to transmit the data between the buoys and a computer on the R/V Savannah.

The UMS system was deployed from the R/V Savannah about 650 m southeast of the R2 navy tower station (27 m regional depth). A tethered buoy was deployed concurrently and, once communication with the UMS was confirmed, the UMS system was released from the vessel. The R/V Savannah's rigid-inflatable boat (RIB) was used to swap the spar buoys and divers periodically inspected the instrument for problems. After 50 hours of operation, the system was recovered and calibrated.

Sampling Methodology. The porewater sampling system was mounted on the deployment frame with the sediment probe's intake filter 4.5 cm from the base of the frame (the predicted sediment interface location). The probe was preprogrammed to sample porewater at depths of 0, 3.8, 5.1, 7.6, 10.2, 12.7, 15.2, and 17.8 cm below the initial position. It was anticipated that the first two sampling depths would be in ambient water and would allow detection of gas concentration gradients above the sediment interface. Sampling depths were referenced to the sediment-water interface. At each position, 2.45 mL were sampled at 0.35 mL/min.

During sampling, porewater traveled from the inlet filter to the membrane in 165 s. However, mixing within the sample tubing, and pervaporation of analyte through the membrane necessitated a six minute signal-stabilization period before measurements were taken. The syringe pump stopped for one minute during the stabilization period while the sediment probe travelled to the next depth. Laboratory observations showed that this procedure reduced the likelihood of clogging the sintered intake filter.

Calibration. The system was calibrated by equilibrating surface water from the R2 site for more than one hour with gas mixtures that contained certified mole fractions of methane, nitrogen, oxygen, argon and carbon dioxide. Sample salinity, measured during sample collection via the research vessel's water sampling system, and sample temperature, measured during sample analysis, allowed calculation of dissolved gas concentrations (Weiss, 1970, 1974; Hamme and Emerson, 2004; Wiesenburg and Guinasso, 1979; Garcia and Gordon, 1992). Gas mole fractions are shown in Table 4. Each sample was analyzed until a stable signal was achieved. The UMS was calibrated for carbon dioxide using only gas mixture 1. Bubbles in the sample line formed

periodically and were flushed out immediately prior to analysis. Blank samples were measured by leaving deionized water in the MIMS assembly with the sample pump inactivated overnight to allow complete degassing of the sample in contact with the membrane. The MIMS assembly temperature was controlled at 45 °C.

Table 4. Standard gas mixtures used for equilibration (in mole fraction).

Gas	Mixture 1	Mixture 2	Mixture 3
Methane	0.00403	0.00501	0.00200
Nitrogen	Balance	Balance	Balance
Oxygen	0.209	0.100	0.180
Argon	0.00768	0.0150	0.00992
Carbon Dioxide	0.000404	0.0020	0.000606

Linear least-squares regressions provided UMS calibration coefficients for methane, nitrogen, oxygen, argon and carbon dioxide concentrations using measured UMS ion currents, I, at *m/z* 15, 28, 32, 40 and 44. I^{44} was also used in the nitrogen regression to account for contributions from carbon dioxide fragmentation. Additionally, all signal intensities were background corrected by subtracting the signal intensity at *m/z* 5, I^5; this subtraction accounts for changes in electronic noise resulting from UMS temperature variability. UMS calibration parameters and deployment parameters were identical: selected ion scan mode; 256 ms dwell time for *m/z* 14, 28, 32, 34, 40, 44, 62; 63 ms dwell time for *m/z* 2, 5, 12, 15, 16, 17, 19, 20, 29, 30, 33, 36, 45, 47, 67, 73, 78, 91, yielding a 3.5 s scan time per cycle; electron multiplier at 1000 V; electron impact energy of 40 eV; 200 mA electron current.

Calibration Correction Terms. Water vapor contributes strongly to MIMS baseline ion currents (Ørsnes et al., 1997). Under hydrostatic pressure, water transmission into the vacuum chamber is significantly reduced (Bell et al., 2007). Therefore, the first calibration coefficient term, β_0 (y-intercept or baseline) was corrected for differences in water vapor contributions between field measurements and calibration. A multiplicative correction factor, CF_{17}, was defined as follows (eq 3.1).

$$\beta_0' = \beta_0 \cdot CF_{17} = \beta_0 \frac{\bar{I}_{cal}^{17}}{I_{field}^{17}} \qquad 3.1$$

Where $\bar{I}_{cal}^{17}$ is the average ion current at *m/z* 17 during calibration, I_{field}^{17} is the ion current at *m/z* 17 during field measurements and β_0' is the corrected first calibration coefficient. β_0' was calculated and applied to each field data point.

The second calibration coefficient term, β_1 (slope or sensitivity), was multiplied by an argon correction term to produce β_1' (eq 3.2).

$$\beta_1' = \beta_1 \cdot CF_{Ar} = \beta_1 \frac{[\mathrm{Ar}]_{sat}}{[\mathrm{Ar}]_{meas}} \qquad 3.2$$

The argon correction term, CF_{Ar}, equal to the ratio of argon saturation concentration, $[\mathrm{Ar}]_{sat}$, to the uncorrected argon concentration measured with the UMS using β_1 and β_0', $[\mathrm{Ar}]_{meas}$. This term accounts for changes in membrane permeability to gases due to hydrostatic pressure. CTD determinations of water temperature and salinity allowed calculation of argon saturation concentrations. CF_{Ar} was generated for each UMS sample taken above the sediment interface, and was interpolated linearly with time for all data points.

Carbon dioxide concentrations were corrected to account for the thermodynamically-induced change in concentration created by the sample temperature difference between in situ or equilibration values and the MIMS measurement value (45 °C) (Guéguen and Tortell, 2008). The alkalinity of the surface seawater, analyzed post-cruise using the spectrophotometric method of Yao and Byrne (1998) was 2380 μmol/kg. Knowing input in situ temperature, salinity, alkalinity and MIMS temperature, MATLAB (Version R2008b; Mathworks, Natwick, MA, USA) scripts adapted to include the CO2SYS program from van Heuven et al. (2009) were used to calculate the change in carbon dioxide concentration. The average equilibration temperature during calibration was 22 °C and the average in situ temperature was 26 °C. The difference between these values resulted in an average correction of 3.5% for in situ data.

Results and Discussion

Porewater Sampling Analysis. Thirty profiles were completed over a period of 54 hours, producing 240 independent sets of gas concentration measurements. Raw UMS data are presented in Figure 12. The stability of the argon data set (I^{40}) indicates that the sample flow rate was constant and bubbles did not form in the sample line during analysis. Bubble formation was mitigated by hydrostatic pressure, and flow rate variability was mitigated through use of the positive displacement syringe pump. Constant sample flow was further ensured through analysis at discrete sample depths. This reduced inlet filter clogging because only small volumes of the sediment column are filtered at discrete depths. However, this added precaution may not be necessary in sediments with percentages of fine grained material as low as are found in the SAB.

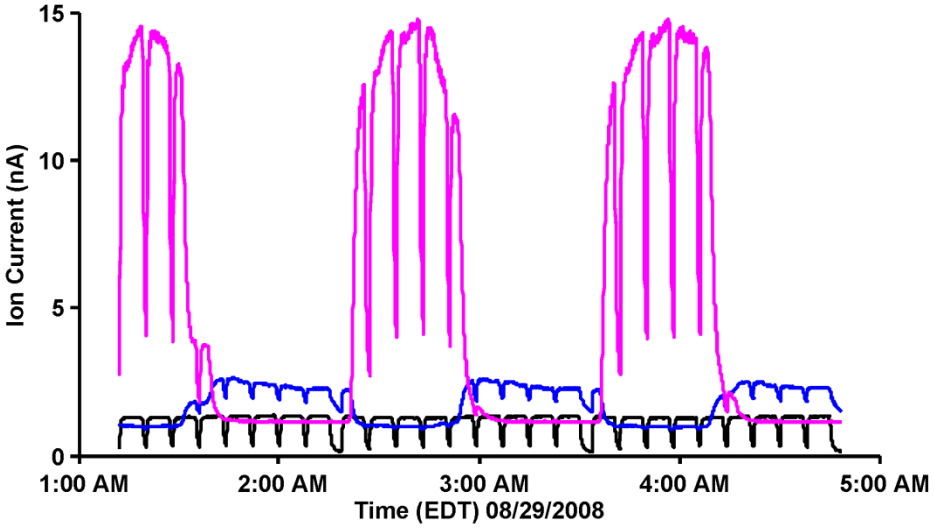

Figure 12. Raw UMS data in time series during three sediment depth profiles. I^{32}, I^{40} , and I^{44} are shown in magenta, black, and blue respectively.

In order to establish the system's ability to define sharp porewater chemoclines it is useful to estimate the system's vertical sampling resolution. Using a sample volume of 2.46 mL and a sediment porosity of 37% (Rao et al., 2007), it was calculated that a 6.6 mL volume of sediment was sampled at each depth. The sampled porewater volume geometries depicted in Figure 13a and 13b were used to estimate the vertical resolution assuming two different torus shaped sampling volumes, a) being the worst case and b) being an optimistic case. Here, the vertical resolution is defined as twice the radius of the toroidal tube representing the porewater volume. Using the probe's outside radius (r_2 = 3.2 mm), the calculated sediment sample volume (V = 6.6 mL), and the two sampling-geometries shown in Figure 13, the estimated vertical sampling resolution was estimated to be between 1.2 and 1.9 cm. In this work, measurement intervals were 2.5 cm; thus a vertical resolution of < 2.0 cm is sufficient to prevent undue smoothing of each depth profile. Though the vertical sampling resolution may be too large to accurately resolve

some sediment porewater gradients, future work and design modifications may enable improved vertical resolutions.

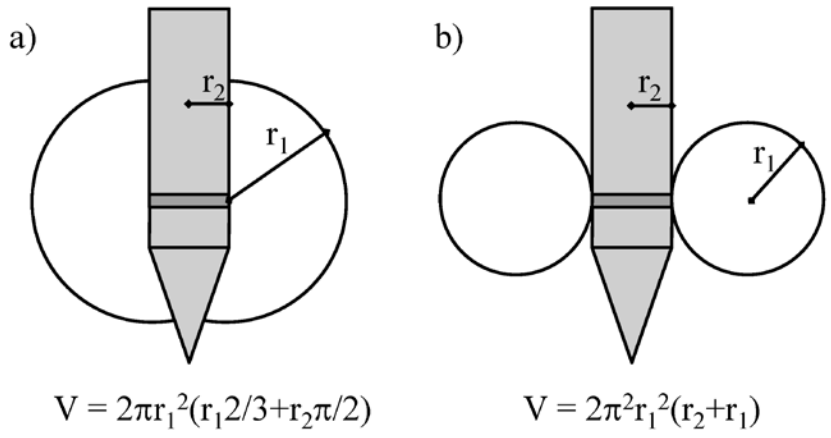

Figure 13. Toroidal models used for estimating sampling resolution shown in 2D. The lightly shaded regions represent the sediment probe, the darkly shaded region represents the sample inlet, and the circular regions represent the volume of porewater sampled. The models were used to constrain estimates of vertical sampling resolutions ($2r_1$) of porewater around the sediment sampling probe.

Local wave-driven redistribution of sediment resulted in oscillations of the sediment interface between 2.8 and 4.0 cm from the probe's initial reference position. Due to the movement of the interface, 24 of the 30 profiles had only a single determination of ambient water concentrations. To avoid spurious interpolations across the sediment interface, the ambient water was assumed to be homogenous. This assumption was confirmed by the 6 profiles that had a second ambient-water determination close to the sediment interface. Sampling depths from each profile were referenced to the sediment-water interface as determined by time-lapse photography.

Each vertical profile was interpolated using a piecewise cubic Hermite algorithm to obtain continuous gas concentration depth profiles for methane, nitrogen, oxygen, argon and carbon dioxide. Concentrations at each depth were then interpolated linearly through time to obtain the data presented as a depth-time contour in Figure 14. Nitrogen

concentrations were divided by argon concentrations to remove the effects of physical processes that would affect nitrogen and argon similarly. For each gas, a chemocline time series was calculated as the depth in the sediment at which the maximum change in concentration occurred.

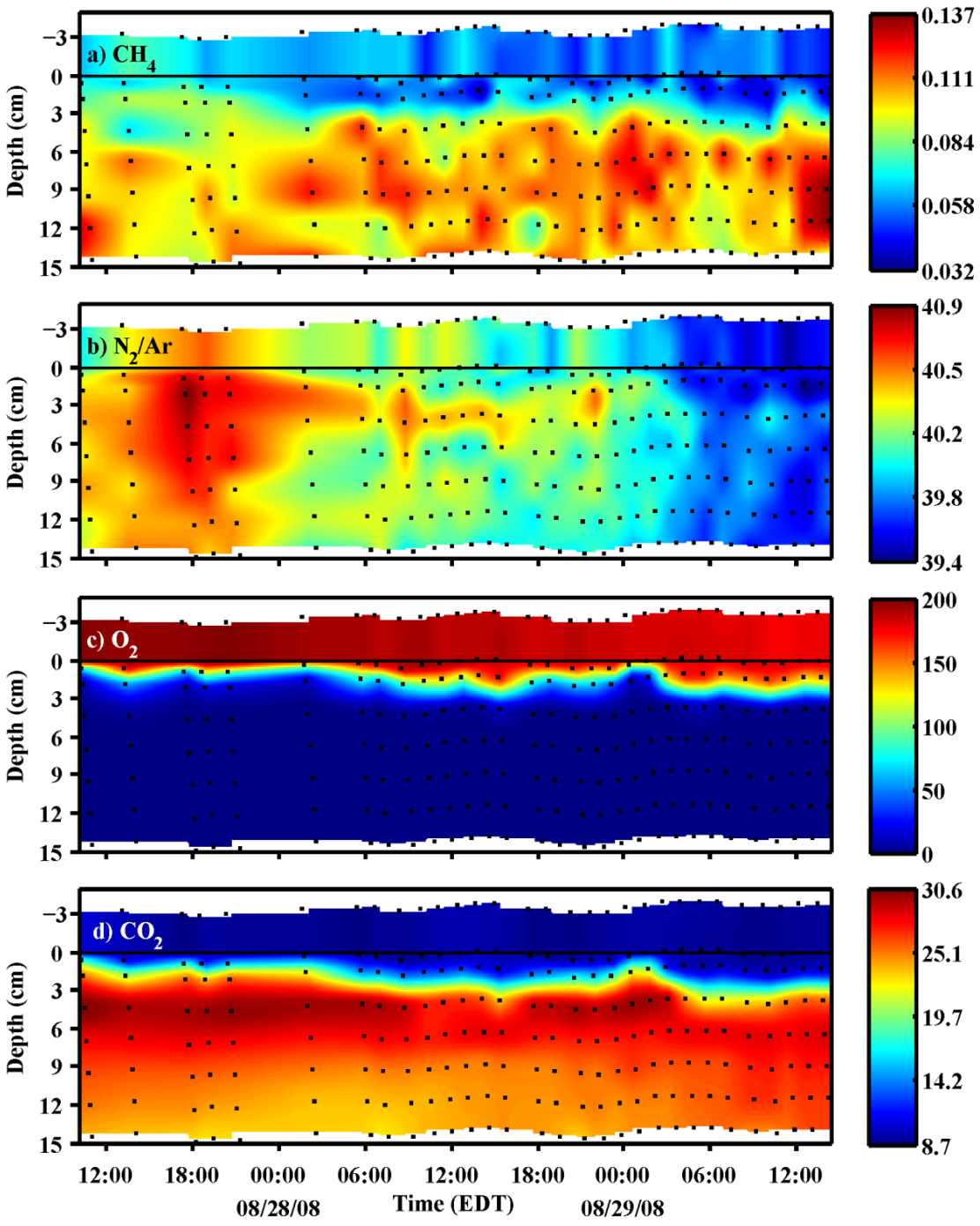

Figure 14. Depth-time contours of calibrated UMS data in sediment porewater. a) Methane concentration (μmol/kg). b) Nitrogen-argon ratio (no units). c) Oxygen concentration (μmol/kg). d) Carbon dioxide concentration (μmol/kg). The horizontal line at 0 cm represents the sediment-water interface as determined by time lapse photography. The '•' markers represent sample locations in time and depth.

Methane concentrations ranging from 0.032 μmol/kg in ambient water to 0.137 μmol/kg in porewater (Figure 14a) indicated the presence of methanogenic bacteria in the sediment. The methane detection limit (three times the standard deviation of the instrumental noise) was determined to be 0.025 μmol/kg. As a result, the methane depth-time contour has substantial uncertainties. Nevertheless, a chemocline is detectable about 3 cm below the sediment interface. Though porewater methane concentrations are low compared to more organic-rich environments (Lloyd et al., 1998), detectable methane concentrations in ambient water suggests that methane production in SAB sediments may be a significant source to the water column. This is consistent with a porewater environment that is dominated by intense metabolic activity and strong advective processes (Janssen et al., 2005; Sansone and Martens, 1981; Jahnke et al., 2005).

Nitrogen-argon ratios data point to active denitrifying-nitrifying biology (Figure 14b). CTD temperature (~26.5 °C) and salinity (~36.0) indicated that nitrogen-argon ratios in ambient water should be between 38.36 and 38.40. Measured values between 39.3 and 40.9 indicate that nitrogen porewater and ambient water concentrations are elevated by 10-20 μmol/kg. The data suggest that increased denitrification occurred on the evening of 08/27/08. The most dynamic region of nitrogen-argon ratios was the suboxic region (~2 cm). This appears to be consistent with the occurrence of denitrification-nitrification across steep redox gradients in suboxic microenvironments (Rao et al., 2008). As these experiments were a first attempt to measure in situ porewater gas concentrations, it was not determined whether a correction for small changes in UMS ionization energy or nitrogen-oxygen interactions is necessary (An et al., 2001). These effects may be contributing to some of the subtle variations detected in the nitrogen-

argon ratio. However, the methods laid out here should enable more precise denitrification estimates in the future.

Oxygen concentrations ranged from 0 μmol/kg below the oxygen chemocline (oxycline) to 200 μmol/kg in the ambient water (Figure 14c). Oxygen determinations using both I^{34} and I^{32} were very closely coupled (data not shown), indicating that hydrogen sulfide, which would have an interfering contribution only at I^{34}, was not present in detectable quantities. Calculated oxygen concentrations at saturation were between 199 and 201 μmol/kg in ambient water. As such, UMS measurements were consistent with ambient water values in near equilibrium with the atmosphere.

Although the carbon dioxide chemocline depth is closely coupled to the oxygen chemocline, on average it was 0.8 cm deeper (Figure 14d). Carbon dioxide concentration maxima were observed at approximately 5.1 cm. The observed maxima point to prevalent methane oxidization and respiration processes. Saturated CO_2^* concentrations (CO_2+H_2CO_3) in ambient water were calculated to vary between 10.2 and 10.4 μmol/kg. UMS results were in agreement with these values.

Oxygen and carbon dioxide chemocline depths were closely coupled in time. The methane chemocline was poorly defined due to similar magnitudes of chemical signals and measurement uncertainties. Nitrogen-argon ratios do not appear to have a clearly defined chemocline. As carbon dioxide had the most distinct chemocline, it was used for comparison with other environmental variables. Carbon dioxide chemocline data are plotted in Figure 15 along with CTD depth (a proxy for tidal height), absorbed photosynthetically active radiation (APAR) (a proxy for photosynthetic production), and

sediment interface depth relative to the probe's initial reference position (a proxy for fine-scale sediment ripple height).

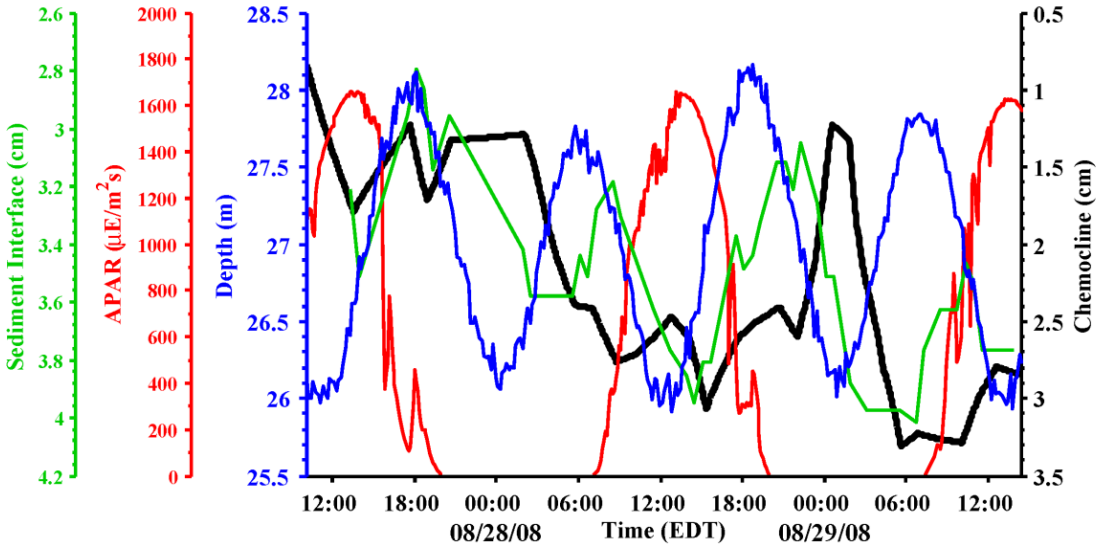

Figure 15. Carbon dioxide chemocline depth time series. Chemocline depth (black) plotted with CTD depth (blue) representing the tidal height, APAR (red) representing, light intensity, and the sediment interface depth (green), which is the distance between the probes starting position and the sediment interface.

A multilinear regression was performed using standardized CTD depth, APAR and sediment interface data, and standardized carbon dioxide chemocline depth as the independent variable. APAR exhibited a relatively low contributing importance to the observed of chemocline depth with a beta coefficient, *b*, equal to 0.26. Tidal height exhibited a medium importance with $b = 0.49$, and sediment interface depth exhibited a relatively strong importance with $b = 0.64$. This suggests that the chemocline depth is predominantly regulated by movement of ripple crests and troughs. This is in agreement with observations (Precht et al., 2004) that changes in advective porewater exchange can be strongly correlated with changes in fine scale sediment topography. Data indicate that

inflow of oxic water into ripple troughs aerates porewater while anoxic upwelling under ripple crests creates a very shallow chemocline.

Conclusions

Sediment porewater dissolved gas concentrations were successfully measured in situ over a 54 hr period in the South Atlantic Bight. Contours of dissolved gas concentrations vs. depth and time were produced for methane, nitrogen-argon ratio, oxygen and carbon dioxide. Methane concentrations were near instrument detection limits, but indicated the presence of methanogenic bacteria in the porewater and elevated concentrations in ambient seawater. Elevated nitrogen-argon ratios suggest that denitrification has a significant impact on porewater nutrient cycling. Concentration profiles for oxygen and carbon dioxide were closely coupled. Subtle changes in chemocline depths were positively correlated with sediment interface depth, suggesting that advective conditions are regulated by ripple topography. These underwater measurements, which constitute the first in situ measurements of dissolved gas porewater profiles by a MIMS system, identify a novel pathway for future in situ porewater analysis.

Chapter 4: In Situ Determination of Total Dissolved Inorganic Carbon by Underwater Membrane Introduction Mass Spectrometry

Abstract

Procedures were developed for determination of total dissolved inorganic carbon (DIC) in acidified seawater using an underwater mass spectrometer. Factors affecting the response of the membrane introduction mass spectrometer (MIMS) system were carefully examined in an effort to optimize calibration procedures and maintain the accuracy and precision required for oceanic carbon system determinations. Laboratory studies examined the following influences on MIMS measurements of DIC: bicarbonate and carbonate contributions to the MIMS CO_2 signal intensity, linearity of MIMS response to carbon dioxide concentration, and the influence of sample salinity on membrane permeability. Results indicate that (a) bicarbonate and carbonate contributions to carbon dioxide signal intensity were significant at slow flow rates, (b) MIMS response was linear to DIC within the concentration range of interest, (c) and salinity has an effect on membrane permeability that is influenced by hydrostatic pressure. A short time-series experiment was performed in Bayboro Harbor, St Petersburg, FL to observe temporal variations in DIC.

Introduction

In the absence of atmospheric/oceanic CO_2 exchange, the atmospheric partial pressure of carbon dioxide (pCO_2) in 2004 would have been 55 ppm higher than observed values near 380 µatm (Sabine et al., 2004). Although oceanic CO_2 uptake is beneficial with respect to removal of greenhouse CO_2 from the atmosphere, the ecological, societal and economic significance of high oceanic pCO_2 is not yet well understood (Doney et al., 2009; Scholes et al., 2009). Facing the prospect of ocean acidification and dramatic climate-change-related decisions based on unreliable and incomplete data, attempts are currently being made to improve the quality and extent of global ocean carbon system observations (Monteiro et al., 2009).

At present, inorganic carbon system species that are commonly measured using laboratory and shipboard methods include pH, alkalinity (A_T), dissolved inorganic carbon (DIC) and carbon dioxide fugacity (fCO_2) (Dickson and Goyet, 1994). Comprehensive inorganic carbon system determinations can be obtained by measuring two or more system parameters (Millero, 2007). In order to minimize problems associated with shipboard and laboratory manual analysis, it is desirable to supplement conventional sampling protocols with in situ sensing techniques. Accordingly, pH and fCO_2 sensors suited for in situ measurements are gaining acceptance in the oceanographic community (Lefèvre et al., 1993; DeGrandpre et al., 1995; Martz et al., 2003; Liu et al., 2006). However, calculation of DIC and A_T using pH-fCO_2 as paired parameters produces uncertainties much larger than state-of-the-art direct measurements (Millero, 2007). As

an alternative to paired pH and fCO_2 parameters, in situ measurements of DIC or A_T can be used to provide compatible analytical pairs: DIC plus either pH or fCO_2 and A_T plus either pH or fCO_2. Consequently, efforts are currently being devoted to measure an expanded set of in situ parameters (Choi et al., 2002; Martz et al., 2006; Byrne and Yao, 2008; Sayles and Eck, 2009).

Membrane introduction mass spectrometers (MIMS) are effective in situ sensors for simultaneous determinations of a wide variety of volatile compounds including CO_2 (Bell et al., 2007; Schlüter and Gentz, 2008; Camilli and Duryea, 2009). MIMS measurements are enabled by gas-permeable membranes, usually polydimethylsiloxane (PDMS), which allow diffusion of gases into a vacuum chamber. The use of MIMS dissolved CO_2 measurements plus potentiometric pH has been demonstrated in laboratory experiments that were focused on non-destructive analysis of small bioreactor samples (Yang et al., 2003; Andersen et al., 2005). The scale of oceanographic measurement, wherein sample volumes are negligible relative to that of the sampled medium, allows for in situ acidification and direct measurements of DIC.

The goal of this work is to understand phenomena that affect MIMS measurements of CO_2 and DIC and, thereby, to provide comprehensive, accurate CO_2-system analysis with a single in situ instrument. To this end, the following questions were addressed in this work: 1) how do CO_2-system equilibria (e.g. $CO_2 + H_2O \leftrightarrow HCO_3^- + H^+$) affect the CO_2 signal intensity in circumneutral seawater solutions? 2) Is MIMS instrument response to dissolved CO_2 linear across the two order of magnitude CO_2 concentration range between circumneutral seawater solutions and acidified seawater solutions? 3) What is the effect of salinity on instrument response? 4) How do in situ

DIC measurements of natural solutions compare to those obtained using a standard discrete sampling technique?

MIMS Carbon System Measurement Theory

pCO_2 Equilibrium. Dissolved CO_2 concentrations in seawater samples can be established by equilibration of seawater with calibrated gas mixtures at a specified temperature, *T*, and salinity, *S*. To avoid evaporative changes in sample salinity and temperature, dry gas can be hydrated by passing the gas stream through water prior to equilibration with samples. The partial pressure of carbon dioxide in a hydrated gas, pCO_2^{wet}, can be calculated from the vapor pressure of H_2O in seawater, pH_2O, and the original carbon dioxide partial pressure of the dry gas, pCO_2^{dry}, using eq 4.1.

$$pCO_2^{wet} = pCO_2^{dry}(1 - pH_2O) \qquad 4.1$$

Water vapor pressure is calculated by methods outlined in Millero et al. (1976). Using pCO_2^{wet} (expressed as a mole ratio) the carbon dioxide fugacity, fCO_2 (expressed in atmospheres), can then be calculated using the Virial equation (Weiss, 1974), expressed in terms of *T* and total pressure, *p*. The solution concentration of carbon dioxide can then be calculated from The Henry's Law constant for CO_2, $K_0^{CO_2}$ (eq 4.2) also given by Weiss (1974) as a function of *T* and *S*.

$$K_0^{CO_2} = \frac{[CO_2]}{fCO_2} \qquad 4.2$$

CO_2 Solution Equilibrium. Dissolved CO_2 reacts with water to produce carbonic acid, H_2CO_3. It is analytically inconvenient to distinguish dissolved CO_2 from H_2CO_3. Therefore they are combined to produce a single parameter, CO_2^* ($[CO_2^*]$ =

$[CO_2] + [H_2CO_3]$). Carbonic acid dissociates to produce bicarbonate, HCO_3^- and carbonate, CO_3^{-2} (eq 4.3 and 4.4) to an extent that is dependent on solution pH. In seawater, the CO_2 system equilibrium constants, K_1' and K_2', are functionally dependent on *S*, *T* and *p*. In this work K_1' and K_2' were taken from Mehrbach et al. (1973) parameterized on the total hydrogen ion scale by Dickson and Millero (1987). Calculations were performed using MATLAB scripts written by the author that incorporate carbon system scripts published by van Heuven et al. (2009). The total pH scale and molinity (mol·kg-soln^{-1}) concentration units were used for carbon system calculations.

$$CO_2^* \leftrightarrows H^+ + HCO_3^- \quad , \qquad K_1' = \frac{[H^+][HCO_3^-]}{[CO_3^{-2}]} \tag{4.3}$$

$$HCO_3^- \leftrightarrows H^+ + CO_3^{2-} \quad , \qquad K_2' = \frac{[H^+][CO_3^{-2}]}{[HCO_3^-]} \tag{4.4}$$

DIC is defined as the sum of all the inorganic carbon species in solution ([DIC] = $[CO_2^*] + [HCO_3^-] + [CO_3^{-2}]$). At a typical surface seawater pH near 8.1 at 25 °C, CO_2^* constitutes less than 0.5% of DIC. At pH 3, 99.9% of DIC is in the form of CO_2^*. Therefore, DIC can be measured by acidifying seawater to a pH below 3.0, whereupon $[CO_2^*]$ can be determined by techniques including coulometry, manometry, spectroscopy and mass spectrometry (Johnson et al., 1993; Guenther et al., 1994; Salata et al., 2000; Byrne et al., 2002; Kaltin et al., 2005).

The activity coefficient, γ, of dissolved CO_2^* in solution increases with ionic strength. The solubility, $\mathbb{S}$, of CO_2 is therefore smaller in seawater than in freshwater (i.e.

$\mathbb{S}_0 \geq \mathbb{S}_{sw}$). The dependence of CO_2 solubility on ionic strength, μ, can be expressed in terms the Setschenow equation (eq 4.5) (Randall and Failey, 1927; Weiss, 1970; Millero, 2000).

$$\ln\left({}^{\mathbb{S}_0}/_{\mathbb{S}_{sw}}\right) = \ln\gamma = k_{\mathbb{S}}\mu \quad , \tag{4.5}$$

where $k_{\mathbb{S}}$ is the salting in (negative) or salting out (positive) coefficient with respect to gas solubility. The ionic strength of seawater can be simulated with NaCl solutions and related to salinity using eq 4.6 (Dickson and Goyet, 1994).

$$m_{NaCl} = \frac{19.924S}{1000 - 1.005S} \tag{4.6}$$

Relation of UMS Signal Intensities to Dissolved Gas Concentrations. MIMS instrument response at a specified mass to charge ratio (*m/z*) is reported as ion current, $I_{m/z}$,. As a measure of instrumental background, *I* at *m/z* = 5 (i.e., I_5) is subtracted from all ion current measurements to account for UMS electronics system temperature fluctuation. As I_5 is negligible for N_2, O_2, Ar and CO_2 determinations, it is not explicitly included in following expressions. Calibration baselines, ${}_G\beta_0$, for gas G, were determined by measuring the sample matrix in the absence of analytes. This condition can be generated by either (a) sparging the solution with a gas, (b) sampling from the solution while it is vigorously boiling, or (c) degassing samples that are in contact with the membrane interface under conditions of no flow (Bell et al., 2007). The analyte sensitivity parameter or slope, ${}_G\beta_1$, is determined by regression analysis of aqueous standards produced by either (a) equilibration of seawater with calibrated gas mixtures, (b) certification of a large batch of samples though conventional analysis or, (c)

quantitative addition of reagents to a blank matrix. Because the baseline intensity is directly determined with a blank measurement, best results are obtained by subtracting baseline values from all subsequent measurements and forcing calibration plots through zero.

As shown by Bell et al. (2007) membrane permeability to water and dissolved gases is affected by hydrostatic pressure. Since water is the primary contributor to baseline signal intensities (Ørsnes et al., 1997), analytical accuracy can be improved by the multiplying calibration baseline values by a water correction factor, CF_{17}, calculated for each field measurement:

$$CF_{17} = \frac{\bar{I}_{17}^{cal}}{I_{17}^{field}} \qquad 4.7$$

Where $\bar{I}_{17}^{cal}$ is the average ion current at *m/z* = 17 during calibration and I_{17}^{field} is the ion current at *m/z* = 17 during field measurements. Thus, UMS field measurements of the dissolved of gas concentrations, $[G]_{meas}$, can be related to instrument response ($I_{m/z}$) using eq 4.8.

$$I_{m/z} = {}_G\beta_1[G]_{meas} + {}_G\beta_0 CF_{17} \qquad 4.8$$

The accuracy of MIMS measurements can occasionally be enhanced through use of an Ar correction factor. Saturated Ar concentrations in seawater can be calculated by measuring salinity and potential temperature and assuming the water sample came into equilibrium with the atmosphere at the measured *S* and potential temperature (Pilson, 1998). Thus, ratios of saturated and UMS-measured Ar concentrations, $[Ar]_{sat}$, and $[Ar]_{meas}$, compensate for changes in analyte sensitivity created by variability in instrument response (eq 4.9).

$$[\mathrm{G}]_{corr} = [\mathrm{G}]_{meas} \frac{[\mathrm{Ar}]_{sat}}{[\mathrm{Ar}]_{meas}} \quad 4.9$$

Examples of parameters that influence instrument response include, temperature, hydrostatic pressure, salinity, and flow rate. By assuming that perturbations in Ar signal intensities are similar to those of other analytes, instrument accuracy can be improved significantly (Kana et al., 1994).

Methods

MIMS System. The UMS system used in this work is based on a previously-published UMS design (Bell et al., 2007) that employs a temperature-regulated flow-through membrane-introduction assembly and PDMS membrane. Significant design modifications relative to the Bell et al. (2007) instrument include the use of a single pressure vessel with all electrical and fluidic feedthroughs on a single endcap, enabling easier access inside the pressure vessel. The roughing pump is currently mounted on vibrational dampeners, and its exhaust (~90% water vapor) is scrubbed with desiccant. Indicating desiccant (Sigma-Aldrich, St Louis, MO) becomes saturated only after months of continuous scrubbing. Therefore, long term deployments are feasible. Further design changes include replacement of fluidic tubing with 1/8" Hastelloy C tubing for additional inertness and use of a fluidic tee that allows two fluid streams to mix before passing over the membrane. Additionally, the sample pump was removed from the UMS pressure vessel. During laboratory-based experiments, sample flow was provided by either an external peristaltic pump (Instech Laboratories, Plymouth Meeting, PA) or an HPLC pump (Hitachi, Japan). During field experiments, sample flow was provided by an underwater syringe pump.

Carbonate Contribution to CO_2 Signal Intensity. To determine the effect of dissolved HCO_3^- and CO_3^{-2} (and other seawater buffering compounds) on the response of the MIMS instrument to CO_2^*, two 1 L seawater samples (S = 36.5 collected from the South Atlantic Bight) were equilibrated with a hydrated air mix (404 ppm pCO_2^{dry}) for over 4 hours. One seawater sample was acidified with 1 mL of 6 M HCl, while the other retained its original alkalinity (A_T = 2390 µmol/kg-soln, determined using the method of Yao et al. (1998)). The two seawater samples and the MIMS assembly were submerged in a 35 °C temperature bath, depicted in Figure 16, Schematic I. Boundary layer depletion-intensity was varied by adjusting sample flow rates between 0 and 16 mL/min during MIMS measurements. This experimental setup is designed to prevent thermally-driven perturbations to carbon system equilibria as demonstrated by Guéguen and Tortell (2008).

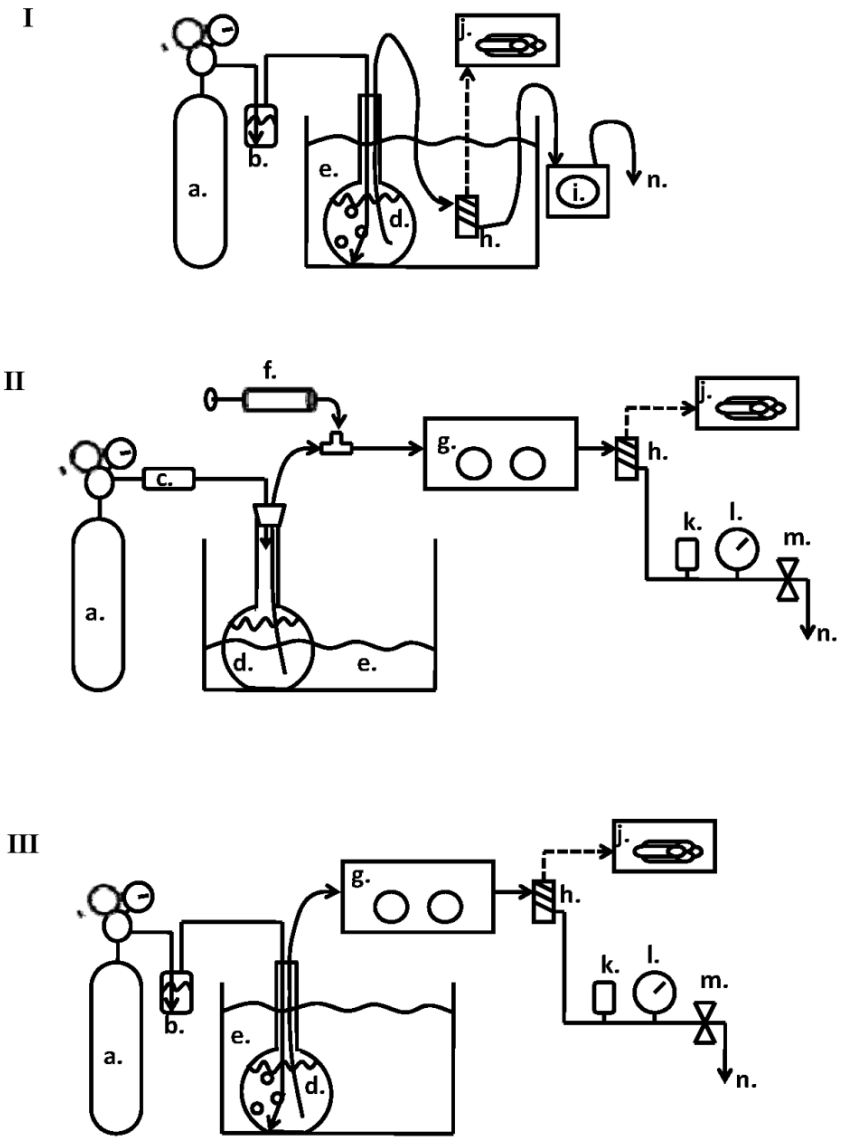

Figure 16. Schematics I, II, and III of laboratory-based experiments. a. Dry gas standard (shown in I-III). b. Gas hydration cell (I, III). c. CO_2 scrubber (II). d. Sample (I-III). e. Constant temperature bath (I-III). f. Reagent addition syringe (II). g. HPLC pump (II-III). h. MIMS Assembly (I-III). i. Peristaltic pump (I). j. Mass Analyzer (I-III). k. Pulse dampener (II-III). l. Pressure gauge (II-III). m. Back pressure regulator (II-III). n. Sample exhaust (I-III).

MIMS DIC Linearity Experiment. DIC standard solutions were generated by gravimetric additions of dried Na_2CO_3 (Sigma-Aldrich, St Louis, MO) to degassed

deionized water (analytical balance model P1-2250, Denver Instruments, Denver, CO). Samples of deionized water (1 L) were purged of CO_2 using N_2 gas scrubbed with NaOH/CaO (Sigma-Aldrich, St Louis, MO). The 1 L flask was then sealed with a Teflon stopper and the total water mass was determined using a calibrated top-loading balance (A&D Weighing, San Jose, CA). NaCl and Na_2CO_3 (Sigma-Aldrich, St Louis, MO) were used to generate solutions with ionic strengths of 0.67 $\mu m \cdot kg\text{-}soln^{-1}$ and various DIC concentrations. The Na_2CO_3 used for standardizations was stored at 150 °C and added gravimetrically while still hot. After complete dissolution of the Na_2CO_3, the resulting sample was partially submerged in a 14 °C bath for 10 to 15 minutes, allowing a thermocline to develop. This ensured that any air contamination would not circulate to the bottom of the sample where the solution was being sampled for MIMS analysis. To prevent inflow of CO_2 into the alkaline standards, the headspace above the solution was flushed with CO_2-free nitrogen gas. A 3.6 M HCl solution (Sigma-Aldrich, St Louis, MO) that had been purged with scrubbed nitrogen gas was injected into the sample stream using a syringe pump (Cole Parmer, Vernon Hills, IL). The sample flow rate was 4 mL/min and the mix ratio was 266:1. A dilution correction was applied to the calculated DIC concentration to account for the acid addition. This experimental setup is depicted in Figure 16, Schematic II. The MIMS assembly was maintained at 35.0 °C, for one dataset and 30 °C for another and an HPLC pump plus a back-pressure regulator were used to maintain hydrostatic pressure at 1.27 atm absolute to reduce bubble formation that can result from increased gas tension at the MIMS assembly during acidification.

MIMS Response to Sample Salinity. The experimental schematic depicted in Figure 16, schematic III, represents the setup for determining the effect of ionic strength (and salinity) on membrane permeability. This setup enables experiments to be performed at elevated hydrostatic pressure. NaCl solutions with ionic strengths equivalent to salinities of 0, 8, 16, 24, 32 and 36 were acidified to pH 2.2. A certified reference standard (CRM #91, S = 33.4) provided by Dr. Andrew Dickson (La Jolla, California) was acidified to pH 2.2. All samples were then simultaneously equilibrated at 23.5 °C with an air mixture containing 990 ppm pCO_2^{dry} and 1% Ar for a minimum of 30 minutes before sampling. Equilibrations continued throughout the experiment. Solutions were generally analyzed three times at a hydrostatic pressure of 184 atm absolute and three times at 1.27 atm absolute. The MIMS assembly was maintained at 35 °C.

In Situ Deployment. For demonstration of in situ capabilities, the UMS was lowered 5.6 m to the seafloor of Bayboro Harbor (St Petersburg, FL). The UMS was mounted on a deployment frame along with an underwater battery, conductivity-temperature-depth (CTD) sensor (RBR Ltd, Ottawa, Canada), and syringe pump system. Continuous power and communication were provided to the instrumentation from shore by a tether. Ethernet communication was routed to the internet, allowing remote data access and commands to the UMS. A 100 µm screen was affixed to the UMS sample inlet, 50 cm from the base of the deployment frame.

During the field deployment, sample flow was provided by the custom-built syringe pump described in Chapter 3. However, the pump was altered by replacing the sediment probe with a 1 mL syringe containing 3.6 M HCl for acidification of the sample

stream. This syringe was equipped with two check valves that enabled periodic replenishment of reagent from a 100 mL acid reservoir that was stored in two 60 mL syringes. Seawater flow rate at 1 mL/min and acid flow rate at 5.0 µL/min created a mixing ratio of 200:1.

Polyurethane tubing (½") fixed to the UMS deployment frame immediately adjacent to the UMS inlet was equipped with a 100 mesh strainer. Harbor water was periodically drawn to shore through the tubing, stored in 500 mL pyrex vessels, and poisoned with 0.2 mL $HgCl_2$ (Sigma-Aldrich, St Louis, MO). The vessels were then sealed with a greased stopper and taped closed. An air bubble (~4 mL) in each vessel permitted temperature-driven changes in sample volume without loss of sample. The samples were stored in a dark, air-conditioned location prior to total carbon analysis for comparison to in situ MIMS results.

Discrete sample analysis was conducted coulometrically (CM5014, UIC Inc, Joliet, IL). Carrier gas, scrubbed of CO_2 by a 40% KOH solution, was used to sparge a 20 mL subsample that was acidified with two 2.5 mL aliquots of 2 N phosphoric acid. The carrier gas was subsequently scrubbed for interfering gases with a 40% KI solution and analyses were conducted in the coulometer's titration cell. Samples were run in duplicate or triplicate. Eight hours of sample analyses were preceded by a blank measurement. A CRM was analyzed after 4 hours, and a second blank was analyzed at the end of 8 hours of analyses. The CRMs were used to ensure measurement consistency and accuracy.

The UMS was also calibrated for DIC with a CRM. For calibration of UMS Ar measurements, two samples of Bayboro Harbor water (S = 32.4) were equilibrated

overnight in a constant temperature bath with two calibrated gas mixtures (Airgas, Radnor, PA). A blank was produced for both Ar and DIC by acidifying a sample of harbor water to pH 2.2, and equilibrating the sample with N_2 gas scrubbed with NaOH/CaO.

Results and Discussion

Carbonate Contribution to CO_2 Signal Intensity. Figure 17 shows CO_2 signal intensities obtained during analysis of acidified and unacidified seawater samples over a range of flow rates. At high flow rates, the closely comparable results obtained using acidified and unacidified samples suggest that the depleted boundary layer behavior at the membrane interface is very similar for the two types of samples. Reductions in ion currents from both samples at low flow rates are attributable to CO_2 depletion in the boundary layer. Under low flow conditions, signal intensities obtained with unacidified sample were systematically higher than those for the acidified sample. Further, the ion currents declined to baseline levels within 10 minutes after sample flow was stopped (flow rate = 0 mL/min) only for the acidified sample. This occurs due to complete degassing of CO_2^* in the membrane boundary layer of the acidified sample. In contrast, the ion currents observed using unacidified samples continued to slowly decrease for more than one hour. In this case, CO_2 was continuously replenished by production of CO_2^* from HCO_3^-.

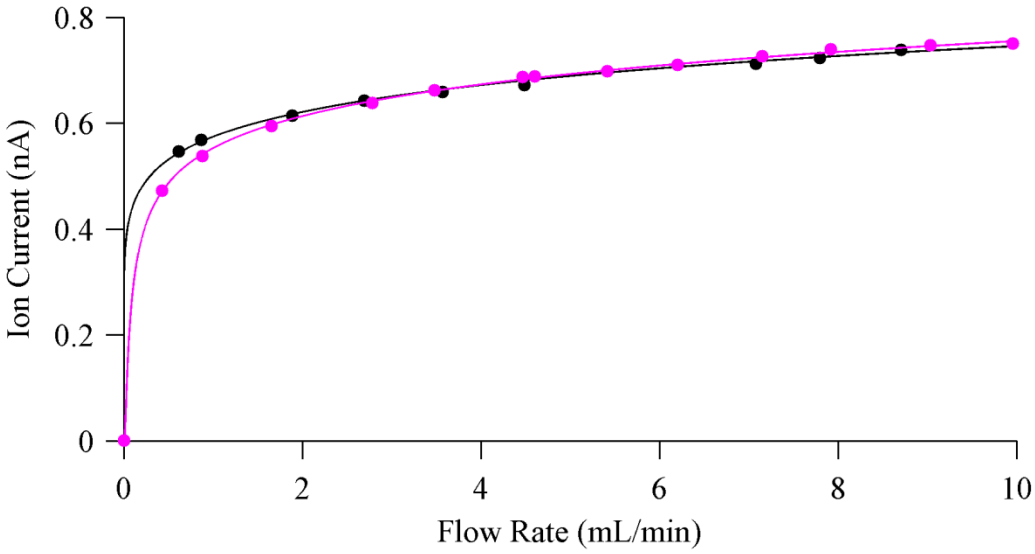

Figure 17. Ion current (I_{44}) vs. sample flow rate. The difference between the unacidified sample (black line) and the acidified sample (red) demonstrates the influence of bicarbonate ions on carbon dioxide signal intensity for the unacidified seawater. Values are baseline subtracted. Solid lines were interpolated using a non-linear fit of the form $I_{44}= \exp(a+b/x +c\ln x)$, where x is flow rate.

In circumneutral solutions ($7 \leq pH \leq 8$), removal of CO_2^* from the membrane/solution boundary layer results in CO_2^* replenishment from the reaction $H^+ + HCO_3^- \rightarrow CO_2 + H_2O$. At a given flow rate, the extent of replenishment will be determined by a sample's buffering intensity and bicarbonate concentration. At slow flow rates this distinction between the behavior of acidified and unacidified solutions confounds comparisons of CO_2^* measurements obtained at different pH or A_T. For measurements at low flow rates, CO_2^* calibrations must be obtained using media that are chemically similar to the expected measurement medium. At high flow rates, CO_2^* replenishment at the membrane boundary layer is not detectable and CO_2-system kinetics (e.g. $H^+ + HCO_3^- \rightarrow CO_2 + H_2O$) are unimportant. At high flow rates CO_2^* calibrations appropriate to circumneutral seawater can be obtained using acidified standards (e.g. Na_2CO_3 standards acidified inline). This is important because preservation issues make the use of CO_2^* standards in circumneutral seawater problematic.

Although carbon system perturbations that result from boundary layer depletion in circumneutral seawater can be minimized through the use of high flow rates, perturbations that result from changes in sample temperature (in situ vs. measured) remain an inherent aspect of UMS analysis. In laboratory work, carbon system thermal effects can be eliminated by maintaining identical membrane temperatures and sample temperatures. In the field, thermal effects can be significant when in situ temperatures are variable. Guéguen and Tortell (2008) showed that carbon system re-equilibrations due to sample temperature perturbations can be addressed through thermodynamic calculations. The CO2SYS software of and Lewis and Wallace (1998) can be used to compensate for this type of thermal perturbation. Though this effect can be minimized by exposing the MIMS membrane to the ambient water during deployment, thermal latency and the influence of temperature on membrane permeability must then be taken into account (Camilli and Duryea, 2009).

MIMS DIC Linearity Experiment. High pCO_2 in compressed gaseous samples can swell PDMS membranes (Royer et al., 1999; Watson and Payne, 1990). Although such effects should be small over the range of CO_2^* concentrations encountered in analysis of acidified and unacidified natural seawater, it is prudent to assess the linearity of instrument response to CO_2 over the relevant range of conditions. Results obtained through online acidification of Na_2CO_3 DIC standards (see Figure 16-III) are shown in Figure 18a. Data sets were collected using membrane temperatures of 30 °C (black circles) and 35 °C (red squares). A baseline measurement was subtracted from all subsequent measurements and the calibration plot was forced through zero. Figure 18b shows the resulting residuals. The skewed distribution of the residuals is suggestive of a

quadratic component in the data. As such, Figure 19a shows the same data set, also baseline subtracted, but fit with a quadratic expression (i.e. DIC = $\beta_1 I_{44} + \beta_2 I_{44}^2$). The residuals shown in Figure 19b exhibit a normal distribution and a significantly improved root mean squared error (RMSE) for the 30 °C dataset relative to the linear fit. The RMSE did not improve for the 35 °C dataset indicating the quadratic fit did not improve the fit as much as would be expected given the reduced degree of freedom. As such, it is presently unclear if the quadratic fit is a better model. Future calibrations should provide additional clarity.

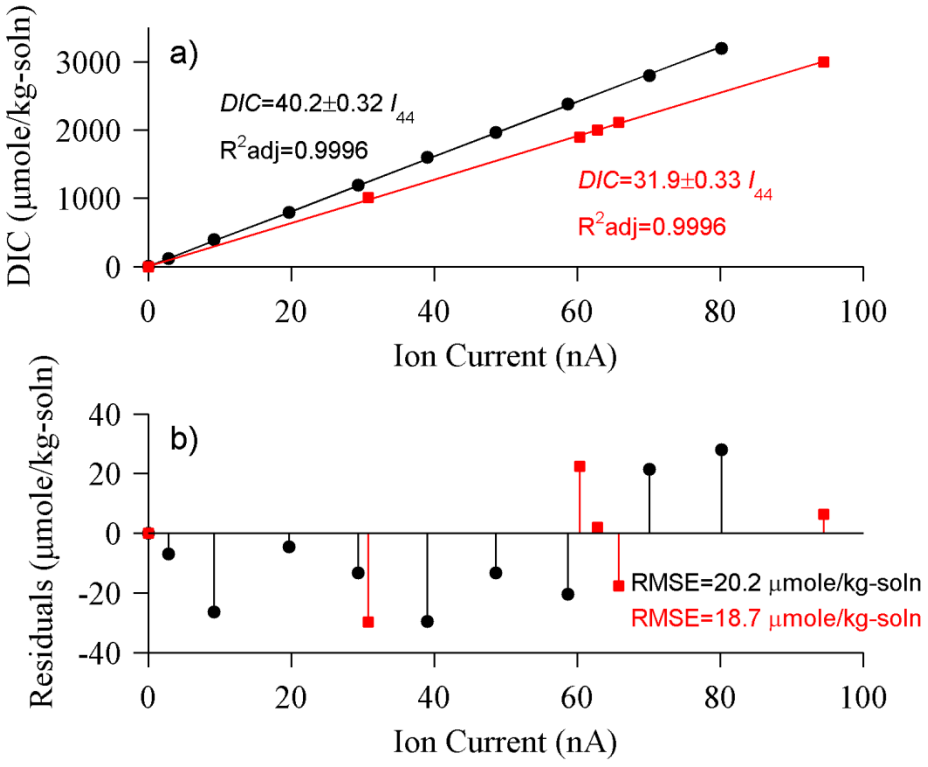

Figure 18. Linear calibration plots using Na_2CO_3 standards acidified inline. Samples represented by black circles were collected using a membrane temperature of 30 °C and red squares represent data collected using a membrane temperature of 35 °C. Data were baseline subtracted, and the linear regression was forced through zero. a) DIC vs. ion current and b) residuals vs. ion current.

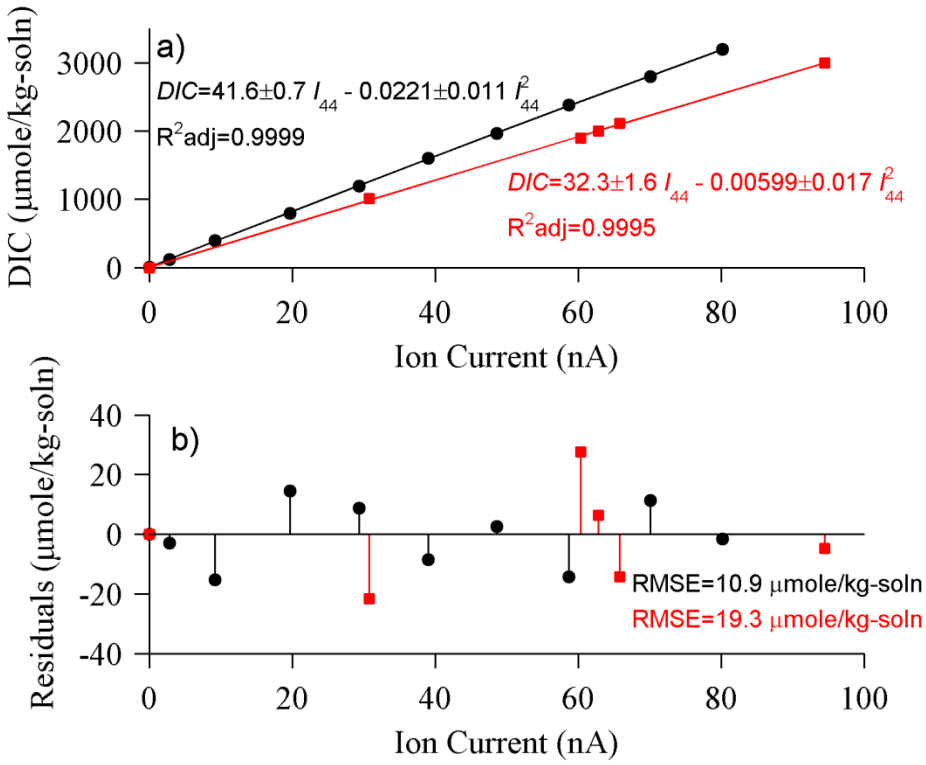

Figure 19. Quadratic calibration plots using Na_2CO_3 standards acidified inline. Samples represented by black circles were collected using a membrane temperature of 30 °C and red squares represent data collected using a membrane temperature of 35 °C. Data were baseline subtracted and fit with a quadratic expression. a) DIC vs. ion current and b) residuals vs. ion current.

MIMS Response to Sample Salinity. Figure 20 shows the results of experiments in which acidified solutions were equilibrated with a calibrated Ar and CO_2 gas mixture and measured with the UMS over a range of ionic strength. As a result of the salting out effect (Weiss, 1974; Millero, 2000), samples bubbled with a given gas mixture have identical fugacities (i.e. *f*Ar and *f*CO_2) but different concentrations (i.e. [Ar] and [CO_2^*]). The ratio of gas phase and solution phase concentrations at a given ionic strength can be described by gas solubility constants via the Setschenow equation (eq 4.5). Expected equilibrium dissolved gas concentrations in Figure 20 are shown in

black. The ratio of gas fugacity in pure water to gas fugacity in NaCl solution is equal to one for all ionic strengths and, as a horizontal line, is not plotted. The ratio of instrument response in pure water ($_{G}I_{0}$) to the response in NaCl solution ($_{G}I_{sw}$) is shown with 68% confidence intervals (red for analysis at 1.27 atm, and in blue for analysis at 184 atm). MIMS data were fit with the Setschenow equation. The instrument responses shown in Figure 20 are intermediate to the expected responses for concentration and fugacity. For both gases it is also observed that increased hydrostatic pressure shifts observed responses toward improved concordance with the response based on fugacity.

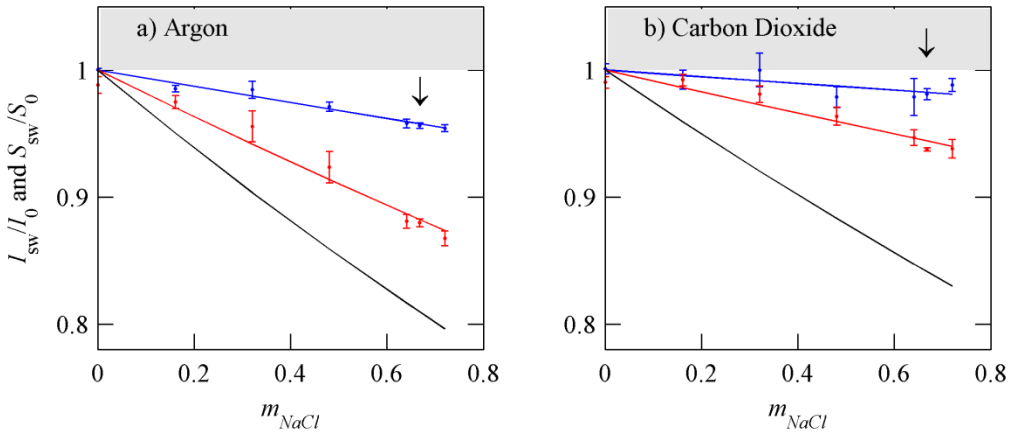

Figure 20. Ion current and sample concentration vs. salinity. Calculated gas concentrations for argon and carbon dioxide are plotted against salinity in black. Ion currents against salinity are presented in red (1.27 atm absolute) and blue (184 atm absolute). Relative gas fugacity is constant (unity) for all salinities. Arrows indicate data obtained from CRM analyses. Good agreement was shown between the CRM and NaCl solutions, indicating NaCl solutions and natural seawater with identical ionic strength produced comparable results.

MIMS instrument response is regulated by membrane permeability, and can be described by a solution-diffusion mechanism (LaPack et al., 1990). This mechanism assumes that partition coefficients, *K*, can be used to describe the chemical equilibria of dissolved gases between the liquid phase and the polymer phase. If it is assumed that

changing instrument response with salinity is a result of a changing membrane partition coefficients and the Setschenow equation adequately describes this change, then salting coefficients can be determined using eq 4.10, where K_0 is the membrane partition coefficient in pure water, K_{sw} is the membrane coefficient in NaCl solution or seawater and k_K is the corresponding membrane salting coefficient. Experimental data are given in Appendix 2 and the resulting salting coefficients are shown in Table 5.

$$\ln\left({}_{G}I_0 \Big/ {}_{G}I_{\mathrm{sw}}\right) = \ln\left(K_0 \Big/ K_{sw}\right) = k_K \mu \qquad 4.10$$

Table 5. Salting coefficients at 35 °C. Membrane salting coefficients, k_K, are presented with 95% confidence intervals. Gas solubility salting coefficients, $k_{\mathbb{S}}$, are also listed.

Gas	k_K (1.27 atm) (kg-H_2O·mol^{-1})	k_K (184 atm) (kg-H_2O·mol^{-1})	$k_{\mathbb{S}}$ - Concentration (kg-H_2O·mol^{-1})	$k_{\mathbb{S}}$ – Fugacity
Ar	0.19±0.02	0.065±0.006	0.32	0
CO_2	0.09±0.01	0.03±0.01	0.26	0

These data suggest that gas pervaporation is driven by two transport mechanisms- one proportional to concentration, the other proportional to fugacity, and the ratio between the two mechanisms is dependent on hydrostatic pressure. At near-atmospheric pressure Ar transport through the membrane is 59% concentration dependent and 41% fugacity dependent. At 184 atm, Ar flux is 21% concentration dependent and 79% fugacity dependent. Similarly, at atmospheric pressure, carbon dioxide flux through the membrane is 35% concentration dependent and 65% fugacity dependent, and at 184 atm flux is 11% concentration dependent and 89% fugacity dependent.

Equilibration-based sensors that employ semi-permeable membranes are responsive to gas fugacities (DeGrandpre et al., 1995; Gouin et al., 1997). Aside from response time, membrane transport behavior in these instruments is not relevant to sensor calibration. MIMS operation is based on measurement of fluxes. Gas concentrations on one side of the membrane are negligible compared to those on the other, and gas fluxes across the membrane are driven by diffusion (Hoch and Kok, 1963). This produces rapid response times and instrument responses that are proportional to membrane permeability.

Prior publications do not provide a definitive account of the effect of salinity on MIMS instrument response. For example, Kasthurikrishnan and Cooks (1995), employing PDMS and microporous Teflon membranes, provided data indicating that instrument response to volatile organic compounds can be proportional to concentration, independent of matrix affects, and salinity variations. The MIMS analyses of Kana et al. (1994) also showed gas transport data (PDMS membrane, O_2, N_2, Ar) that were proportional to dissolved gas concentrations. However, the observed instrument responses to changes in salinity between of 0 and 36 in the work of Kana et al. (1994) had a systematic deviation from the expected concentration-based response by about 5%. This observation and the results shown in Figure 20 suggest that gas transport through PDMS membranes may be more complicated than has been previously supposed. Further, the work of de Vos Petersen et al. (2004) showed that salinity exerted a strong influence on instrument response to methyl-branched aldehydes. In support of the observations shown in Figure 20, the observations of de Vos Petersen et al. (2004) indicate that some portion of the transport behavior of PDMS membranes is proportional to analyte fugacity rather than analyte concentration.

Use of Standard Reference Materials in MIMS Analysis. Procedures for producing reliable Na_2CO_3 standards for DIC determinations are inconvenient for shipboard use. Consequently, CRMs have become a widely used to ensure the reliability of carbon system data (Lamb et al., 2001). These reference standards, composed using Pacific Ocean seawater, generally have salinities between 33 and 34. If CRMs are used for calibration, salinity correction factors (CF_{Sal}) are needed for samples that have a range of salinities. Using eqs 4.11 and 4.6, the ion current for a given gas, ${}_{G}I$, at a given hydrostatic pressure can be corrected to account for variations in salinity to yield ${}_{G}I_{conc}$, which is the ion current expressed proportionally to gas concentration.

$$ {}_{G}I_{conc} = {}_{G}I * CF_{Sal} = {}_{G}Ie^{(k_{\mathbb{S}}-k_K)m_{NaCl}} \qquad 4.11 $$

If the instrument is calibrated using standards with salinities approximately equal to the salinity of each field sample, the correction terms (e.g. CF_{Sal} for the calibration standards and $CF_{Sal}$for the field samples) will cancel and salinity corrections are negligible. However, as an example, if the difference between standard and sample salinities varies by 10 units, the resulting fugacity correction factor CF_{Sal}, will be 0.97 for carbon dioxide. As such, this is a substantial effect that must be considered.

Since the salinity correction factors must be applied to both argon and carbon dioxide signal intensities, and the magnitude of each correction is similar, it may be appropriate to obtain salinity corrections simply by normalizing with the argon signal (eq 4.9). This correction also accounts for variations in signal intensity that result from changes in membrane temperature, hydrostatic pressure, and membrane conditions. In this case it is assumed that each parameter affects carbon dioxide and argon signal intensities equally. Best results from this method would be obtained using standards

containing known concentrations of both Ar and DIC in order to as to produce simultaneous Ar and DIC calibrations. Measurement errors attributed to fluctuating analysis conditions (as listed above) will then largely cancel. Similarly, field measurement of Ar and DIC should be concurrent. At present, a means of producing (or certifying) standards for concurrent measurements of Ar and DIC concentrations has not been identified.

Predictions of oceanic Ar concentrations can be made based on solubility behavior (Pilson, 1998). However, Ar concentrations in seawater are influenced by a number of non-thermodynamic processes (e.g. bubble injection, thermal perturbation or bubble exchange (Leifer and Patro, 2002; Emerson and Hedges, 2008)). Under these circumstances corrections using Ar normalizations would not appropriately account for all processes that influence the comparative transport behavior of Ar and CO_2. As such, direct corrections for salinity (eq 4.11) and pressure (Chapter 2, eq 2.7) would be required.

In Situ Deployment. DIC data were collected in Bayboro harbor over a period of 68 hours, and samples were drawn periodically for coulometric DIC analysis (Figure 21). Since the salinity of the CRM used for UMS calibration was within one unit of the in situ water being analyzed ($33.2 \leq S \leq 32.3$) and the UMS depth was less than six meters, pressure and salinity correction factors were very small. However, UMS results were in poor agreement with coulometry data until the Ar correction method was applied (eq 4.9). The magnitude of the offset between the UMS and coulometry DIC analyses, even with Ar normalization, points to the need for improved UMS accuracy. Observations of seawater density (calculated from temperature and salinity) demonstrate

the existence of high frequency changes in water conditions that are not resolved by either the discrete coloumetric data or the in situ UMS data. A diurnal trend is not observed in either the MIMS DIC data or the coulometric DIC data. Nor did a severe rain event that occurred on the evening of 05/17/09 produce an observable DIC response.

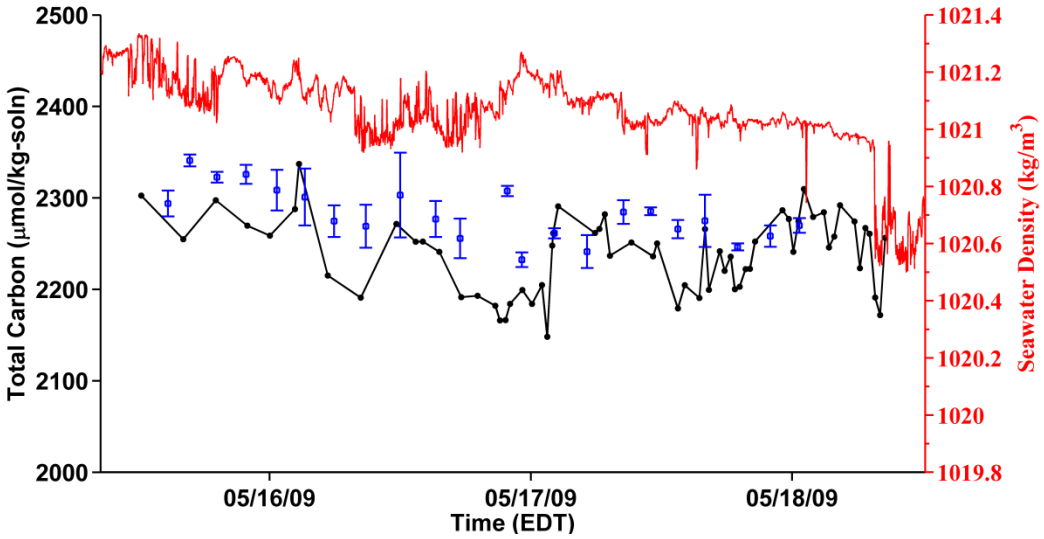

Figure 21. DIC as measured by the UMS and by coulometry. The black line represents DIC collected via UMS, and the blue squares represent discrete coulometric samples with 95% confidence intervals. Red data represent seawater density. The mean absolute error between the in situ UMS data and discrete coulometric data is 43 µmol/kg-soln.

It was expected that the hydrostatic pressure at ~6 m depth would preclude gas supersaturation and bubble formation subsequent to acidification at 35 °C. However, sudden spurious changes in MIMS ion currents indicated the formation of bubbles in the sample line. Consequently, the routine controlling the syringe pump was modified in situ: the continuous pumping protocol was changed to a discrete sampling protocol that included a flushing stage. Samples were drawn at 7 mL/min for 30 seconds with a corresponding increase in acid flow to flush the system of bubbles, and then flow was set to 1 mL/min for 28 minutes during analysis. Data were collected 5 to 10 minutes after

the flush, allowing time for the membrane temperature to stabilize after the sudden changes in flow rate.

The occurrence of bubbles in the sample line is attributed to negative head pressure produced by drawing (instead of pushing) the sample through the MIMS assembly. As a result of the described problems with bubbles, analytical accuracy and sampling frequency did not match the measurement capabilities that had been demonstrated in the laboratory. Future work will focus on improvement of field DIC accuracy through modifications to the sampling methodology, and through periodic sampling of an in situ standard. It would also be advantageous for future deployments to occur at depths on the order of ten to more meters.

Conclusions

Determinations of DIC by MIMS were found to be largely linear over a wide range of concentrations. However, measurement accuracy was somewhat improved by inclusion of a very small quadratic term. Contributions to CO_2 signal intensity from HCO_3^- and CO_3^{-2} occurred at low flow rates. This effect, which resulted from depleted boundary layer conditions, was virtually undetectable at higher sample flow rates. Flow rate effects thus need to be taken into consideration when MIMS instruments are calibrated for pCO_2 measurements. MIMS response to CO_2 and Ar is dependent on salinity, and the extent of the salinity dependence is affected by hydrostatic pressure. The effect of salinity on MIMS response can be modeled by calibration over a wide range of salinities or, alternatively, minimized through use of Ar normalization.

Although additional work is needed before MIMS instruments are capable of examining the marine CO_2 system with state of the art accuracy and precision, the ability

to make simultaneous measurements of pCO_2, DIC and other important marine analytes (i.e. CH_4, N_2, O_2, H_2S, Total Sulfide, Ar and DMS) makes the UMS a uniquely capable instrument. Simultaneous detection of these analytes using a single in situ sensor provides a novel approach toward comprehensive understanding of the biogeochemical processes that regulate our oceans.

Summary

Sustained ocean observations with high spatial and temporal resolution require robust in situ instrumentation. To meet the requirements of modern research, quantification procedures and performance of in situ instruments must be carefully documented. As such, the behavior of underwater membrane introduction mass spectrometers developed at the University of South Florida and SRI International were characterized with respect to the influences of sample hydrostatic pressure, salinity, flow rate, and chemistry. These characterizations enabled the collection of quantified dissolved gas profiles in the Gulf of Mexico to depths of 500 m. Development of a sediment probe/syringe pump system enabled repeated analysis of sediment porewater dissolved gas concentration profiles at 27 m depth in the South Atlantic Bight over a 54 hour period. Further broadening the applications of underwater membrane introduction mass spectrometer systems, measurements of total dissolved inorganic carbon (DIC) were demonstrated by means of inline sample acidification. DIC measurements of acidified seawater in conjunction with CO_2 measurements in unacidified seawater allow comprehensive determinations of the marine carbon system using two compatible carbon system variables with a single instrument. The measurements described in this dissertation constitute the first quantitative observations of dissolved gas ocean profiles, sediment porewater profiles, and DIC measurements by underwater mass spectrometry.

References Cited

An S, Gardner WS, and Kana T. 2001. Simultaneous measurement of denitrification and nitrogen fixation using isotope pairing with membrane inlet mass spectrometry analysis. *Appl. Environ. Microbiol. 67*(3), 1171-1178. doi:10.1128/AEM.67.3.1171-1178.2001.

Andersen AZ, Lauritsen FR, and Olsen LF. 2005. On-line monitoring of CO2 production in Lactococcus lactis during physiological pH decrease using membrane inlet mass spectrometry with dynamic pH calibration. *Biotechnol. Bioeng. 92*(6), 740-747. doi:10.1002/bit.20641.

Bell RJ, Short RT, van Amerom FHW, and Byrne RH. 2007. Calibration of an in situ membrane inlet mass spectrometer for measurements of dissolved gases and volatile organics in seawater. *Environ. Sci. Technol. 41*(23), 8123-8128. doi:10.1021/es070905d.

Bell RJ, Toler SK, van Amerom FH, Wenner PG, Hall M, Edkins JE, Gassig S, Short RT, and Byrne RH. 2004. Measurement of relative dissolved gas concentrations using underwater mass spectrometry. In: *Eos Trans. AGU*, 85(47), Fall Meet. Suppl., Abstract OS13B-0532.

Benstead J, and Lloyd D. 1994. Direct mass spectrometric measurement of gases in peat cores. *FEMS Microbiol. Ecol. 13*(3), 233-240. doi:10.1111/j.1574-6941.1994.tb00070.x.

Bossuyt A, and McMurtry G. 2004. A deep-sea mass spectrometer instrument for long-term, in situ biogeochemical monitoring. 85(47), Fall Meet. Suppl., Abstract OS43B-0555.

Byrne RH, Liu X, Kaltenbacher EA, and Sell K. 2002. Spectrophotometric measurement of total inorganic carbon in aqueous solutions using a liquid core waveguide. *Anal. Chim. Acta 451*(2), 221-229. doi:10.1016/S0003-2670(01)01423-4.

Byrne RH, and Yao W. 2008. Procedures for measurement of carbonate ion concentrations in seawater by direct spectrophotometric observations of Pb(II) complexation. *Mar. Chem. 112*(1-2), 128-135. doi:10.1016/j.marchem.2008.07.009.

Camilli R, and Hemond H. 2004. NEREUS/Kemonaut, a mobile autonomous underwater mass spectrometer. *TrAC, Trends Anal. Chem. 23*(4), 307-313.

Camilli R, and Duryea AN. 2009. Characterizing spatial and temporal variability of dissolved gases in aquatic environments with in situ mass spectrometry. *Environ. Sci. Technol. 43*(13), 5014-5021. doi:10.1021/es803717d.

Choi YS, Lvova L, Shin JH, Oh SH, Lee CS, Kim BH, Cha GS, and Nam H. 2002. Determination of oceanic carbon dioxide using a carbonate-selective electrode. *Anal. Chem. 74*(10), 2435-2440. doi:10.1021/ac0108459.

Conrad R. 1996. Soil microorganisms as controllers of atmospheric trace gases (H2, CO, CH4, OCS, N2O, and NO). *Microbiol. Rev. 60*(4), 609-640.

Cornwell JC, Kemp WM, and Kana TM. 1999. Denitrification in coastal ecosystems: methods, environmental controls, and ecosystem level controls, a review. *Aquat. Ecol. 33*(1), 41-54. doi:10.1023/A:1009921414151.

Crank J. 1975. *The mathematics of diffusion*. Clarendon Press, Oxford.

DeGrandpre MD, Hammar TR, Smith SP, and Sayles FL. 1995. In situ measurements of seawater pCO2. *Limnol. Oceanogr. 40*(5), 969-975.

Dickens GR, Paull CK, and Wallace P. 1997. Direct measurement of in situ methane quantities in a large gas-hydrate reservoir. *Nature 385*(6615), 426-428. doi:10.1038/385426a0.

Dickson AG, and Goyet C. 1994. Handbook of methods for the analysis of the various parameters of the carbon dioxide system in sea water. Version 2. ORNL/CDIAC-74. . doi:10.2172/10107773.

Dickson AG, and Millero FJ. 1987. A comparison of the equilibrium constants for the dissociation of carbonic acid in seawater media. *Deep Sea Res. 34*(10), 1733-1743. doi:10.1016/0198-0149(87)90021-5.

Doney SC, Fabry VJ, Feely RA, and Kleypas JA. 2009. Ocean acidification: The other CO2 problem. *Annu. Rev. Marine. Sci. 1*(1), 169-192. doi:10.1146/annurev.marine.010908.163834.

Emerson S, and Hedges J. 2008. *Chemical Oceanography and the Marine Carbon Cycle*. Cambridge University Press.

Ersland G, Husebø J, Graue A, and Kvamme B. 2009. Transport and Storage of CO2 in Natural Gas Hydrate Reservoirs. *Energy Procedia 1*(1), 3477-3484. doi:doi:10.1016/j.egypro.2009.02.139.

Eyre B, Rysgaard S, Dalsgaard T, and Christensen P. 2002. Comparison of isotope pairing and N2:Ar methods for measuring sediment denitrification—Assumption, modifications, and implications. *Estuaries and Coasts 25*(6), 1077-1087. doi:10.1007/BF02692205.

Favre E, Schaetzel P, Nguygen Q, Clement R, and Neel J. 1994. Sorption, diffusion and vapor permeation of various penetrants through dense polydimethylsiloxane membranes: a transport analysis. *J. Membr. Sci. 92*, 169-184.

Fujita H. 1961. Diffusion in polymer-diluent systems. *Algebra Univ. 3*(1), 1-47.

Futo I, and Degn H. 1994. Effect of sample pressure on membrane inlet mass spectrometry. *Anal. Chim. Acta 294*(2), 177-184.

Garcia HE, and Gordon LI. 1992. Oxygen solubility in seawater: better fitting equations. *Limnol. Oceanogr. 37*(6), 1307-1312.

Gereit F, Hauptmann P, Matz G, Mellert V, and Reuter R. 1998. An ROV-based sensor system for maritime pollution control. In: *Ocean. Int. 98,* Brighton, UK.

Gorsline DS. 1963. Bottom sediments of the Atlantic Shelf and Slope off the southern United States. *J. Geol. 71*(4), 422-440.

Gouin J, Baros F, Birot D, and André J. 1997. A fibre-optic oxygen sensor for oceanography. *Sens. Actuators, B 39*(1-3), 401-406. doi:10.1016/S0925-4005(97)80242-0.

Guéguen C, and Tortell P. 2008. High-resolution measurement of Southern Ocean CO2 and O2/Ar by membrane inlet mass spectrometry. *Mar. Chem. 108*(3-4), 184-194. doi:10.1016/j.marchem.2007.11.007.

Guenther P, Keeling CD, and Emanuele III G. 1994. *Oceanic CO2 measurements for the WOCE hydrographic survey in the Pacific Ocean, 1990--1991: shore based analyses*.

Hamme R. 2006. Gas Solubility Matlab Functions. Available from: http://web.uvic.ca/~rhamme/download.html

Hamme RC, and Emerson SR. 2002. Mechanisms controlling the global oceanic distribution of the inert gases argon, nitrogen and neon. *Geophys. Res. Lett. 29*(23), 35-1.

Hamme RC, and Emerson SR. 2004. The solubility of neon, nitrogen and argon in distilled water and seawater. *Deep Sea Res. Part I 51*(11), 1517-1528. doi:10.1016/j.dsr.2004.06.009.

Hansen KF, and Degn H. 1996. On-line membrane inlet mass spectrometry for feed-back control of precursor concentration in penicillin fermentation. *Biotechnol. Tech. 10*(7), 485-490. doi:10.1007/BF00159511.

Hansen KF, Gylling S, and Lauritsen FR. 1996. Time- and concentration-dependent relative peak intensities observed in electron impact membrane inlet mass spectra. *Int. J. Mass Spectrom. Ion Processes 152*(2-3), 143-155. doi:10.1016/0168-1176(95)04338-1.

Hartnett HE, and Seitzinger SP. 2003. High-resolution nitrogen gas profiles in sediment porewaters using a new membrane probe for membrane-inlet mass spectrometry. *Mar. Chem. 83*(1-2), 23-30. doi:10.1016/S0304-4203(03)00093-8.

Harvey F. 1974. High temperature oxidation of tungsten wires in water vapor-argon mixtures. *Metall. Trans. 5*, 1189-1192.

Hemond H, and Camilli R. 2002. NEREUS: engineering concept for an underwater mass spectrometer. *TrAC, Trends Anal. Chem. 21*(8), 526-533. doi:10.1016/S0165-9936(02)00113-9.

van Heuven S, Pierrot D, Lewis E, and Wallace D. 2009. *MATLAB program developed for CO2 system calculations. ORNL/CDIAC-105b.* Carbon Dioxide Information Analysis Center, Oak Ridge National Laboratory, U.S. Department of Energy, Oak Ridge, Tennessee.

Hoch G, and Kok B. 1963. A mass spectrometer inlet system for sampling gases dissolved in liquid phases. *Arch. Biochem. Biophys 101*, 160-170.

Hoffmann ED, and Stroobant V. 2007. *Mass Spectrometry: Principles and Applications*. 3rd ed. Wiley-Interscience.

Jahnke R, Richards M, Nelson J, Robertson C, Rao A, and Jahnke D. 2005. Organic matter remineralization and porewater exchange rates in permeable South Atlantic Bight continental shelf sediments. *Cont. Shelf Res. 25*(12-13), 1433-1452. doi:10.1016/j.csr.2005.04.002.

Janfelt C, Frandsen H, and Lauritsen FR. 2006. Characterization of a mini membrane inlet mass spectrometer for on-site detection of contaminants in both aqueous and liquid organic samples. *Rapid Commun. Mass Spectrom. 20*(9), 1441-1446. doi:10.1002/rcm.2466.

Janssen F, Huettel M, and Witte U. 2005. Pore-water advection and solute fluxes in permeable marine sediments (II): benthic respiration at three sandy sites with different permeabilities (German Bight, North Sea). *Limnol. Oceanogr. 50*(3), 779-792.

Johnson K, Wills K, Butler D, Johnson W, and Wong C. 1993. Coulometric total carbon dioxide analysis for marine studies: maximizing the performance of an automated gas extraction system and coulometric detector. *Mar. Chem. 44*(2-4), 167-187. doi:10.1016/0304-4203(93)90201-X.

Johnson RC, R. G. Cooks, T. M. Allen, M. E. Cisper, and P. H. Hemberger. 2000. Membrane introduction mass spectrometry: Trends and applications. *Mass Spectrom. Rev. 19*(1), 1-37. doi:10.1002/(SICI)1098-2787(2000)19:1<1::AID-MAS1>3.0.CO;2-Y.

Kaltin S, Haraldsson C, and Anderson LG. 2005. A rapid method for determination of total dissolved inorganic carbon in seawater with high accuracy and precision. *Mar. Chem. 96*(1-2), 53-60. doi:10.1016/j.marchem.2004.10.005.

Kamiya Y, Naito Y, Terada K, and Mizoguchi K. 2000. Volumetric properties and interaction parameters of dissolved gases in poly(dimethylsiloxane) and polyethylene. *Macromolecules 33*(8), 3111-3119.

Kana T, Weiss D, Eyre B, Rysgaard S, Dalsgaard T, and Christensen P. 2004. Comment on: "Comparison of isotope pairing and N2:Ar methods for measuring sediment denitrification" by Eyre, B.D. et al. Authors' reply. *Estuaries 27*(1), 173-178.

Kana TM, Darkangelo C, Hunt MD, Oldham JB, Bennett GE, and Cornwell JC. 1994. Membrane inlet mass spectrometer for rapid high-precision determination of N2, O2, and Ar in environmental water samples. *Anal. Chem. 66*(23), 4166-4170. doi:10.1021/ac00095a009.

Kana TM, Sullivan MB, Cornwell JC, and Groszkowski KM. 1998. Denitrification in estuarine sediments determined by membrane inlet mass spectrometry. *Limnol. Oceanogr. 43*(2), 334-339. doi:10.2307/2839221.

Kasthurikrishnan N, and Cooks RG. 1995. On-line flow injection analysis of volatile organic compounds in seawater by membrane introduction mass spectrometry. *Talanta 42*(9), 1325-1334. doi:10.1016/0039-9140(95)01588-3.

Ketola RA, Virkki VT, Ojala M, Komppa V, and Kotiaho T. 1997. Comparison of different methods for the determination of volatile organic compounds in water samples. *Talanta 44*(3), 373-382. doi:10.1016/S0039-9140(96)02072-3.

Kibelka G, Hadjar H, Shill S, Kassan S, Camercon C, and Brown T. 2009. Compact GC/MS based on the ion-camera mass spectrometer. Available from: http://www.pittcon.org/technical/finalprogram.html

Klimant I, Meyer V, and Kuhl M. 1995. Fiber-optic oxygen microsensors, a new tool in aquatic biology. *Limnol. Oceanogr. 40*(6), 1159-1165.

Klopffer M, and Flaconneche B. 2001. Transport properties of gases in polymers: bibliographic review. *Oil Gas Sci. Technol. 56*(3), 223-244.

Kotiaho T. 1996. On-site environmental and in situ process analysis by mass spectrometry. *J. Mass Spectrom. 31*(1), 1-15. doi:10.1002/(SICI)1096-9888(199601)31:1<1::AID-JMS295>3.0.CO;2-J.

Krogh ET, van Pel DM, Lynch MS, Gill CG, Durning CJ, and Janes D. 2006. Measurement of environmentally relevant partition and diffusion coefficients using membrane introduction mass spectrometry. In: *54th ASMS Conference Proceedings*. Available from: http://md1.csa.com/partners/viewrecord.php?requester=gs&collection=TRD&recid=20070917143848SO

Lamb MF, Sabine CL, Feely RA, Wanninkhof R, Key RM, Johnson GC, Millero FJ, Lee K, Peng T-, Kozyr A, et al. 2001. Consistency and synthesis of Pacific Ocean CO2 survey data. *Deep Sea Res. Part II 49*(1-3), 21-58. doi:10.1016/S0967-0645(01)00093-5.

LaPack MA, Tou JC, and Enke CG. 1990. Membrane mass spectrometry for the direct trace analysis of volatile organic compounds in air and water. *Anal. Chem. 62*(13), 1265-1271. doi:10.1021/ac00212a013.

LaPack MA. 1995. The theory and practice of membrane extractions. Ph.D. Thesis, 198 pp., Michigan State University.

Lapham LL, Alperin M, Chanton J, and Martens C. 2008. Upward advection rates and methane fluxes, oxidation, and sources at two Gulf of Mexico brine seeps. *Mar. Chem. 112*(1-2), 65-71. doi:10.1016/j.marchem.2008.06.001.

Lauritsen FR, and Gylling S. 1995. Online monitoring of biological reactions at low parts-per-trillion levels by membrane inlet mass spectrometry. *Anal. Chem. 67*(8), 1418-1420. doi:10.1021/ac00104a018.

Lauritsen FR, Jensen A, and Nielsen CH. 2008. Fast and direct screening of solid materials for their potential liberation of hydrophobic organic compounds using hot cell membrane inlet mass spectrometry. *Rapid Commun. Mass Spectrom. 22*(14), 2234-2240. doi:10.1002/rcm.3608.

Lauritsen FR, Kotiaho T, Choudhury TK, and Cooks RG. 1992. Direct detection and identification of volatile organic compounds dissolved in organic solvents by reversed-phase membrane introduction tandem mass spectrometry. *Anal. Chem. 64*(11), 1205-1211. doi:10.1021/ac00035a003.

Lefèvre N, Ciabrini JP, Michard G, Brient B, DuChaffaut M, and Merlivat L. 1993. A new optical sensor for PCO2 measurements in seawater. *Mar. Chem. 42*(3-4), 189-198. doi:10.1016/0304-4203(93)90011-C.

Leifer I, and Patro RK. 2002. The bubble mechanism for methane transport from the shallow sea bed to the surface: A review and sensitivity study. *Cont. Shelf Res. 22*(16), 2409-2428. doi:10.1016/S0278-4343(02)00065-1.

Lennemann F. 1999. Membrane inlet mass spectrometry for bioreactors-modelling and application for gases and liquids. Ph.D. Thesis, Hamburg-Harburg Technical University.

Lewis E, and Wallace DWR. 1998. *Program developed for CO2 system calculations. ORNL/CDIAC-105*. Carbon Dioxide Information Analysis Center, Oak Ridge National Laboratory, U.S. Department of Energy, Oak Ridge, Tennessee.

Lipnizki F, and Trägårdh G. 2001. Modelling of pervaporation: Models to analyze and predict the mass transport in pervaporation. *Sep. Purif. Methods 30*(1), 49-125. doi:10.1081/SPM-100102985.

Liu X, Wang ZA, Byrne RH, Kaltenbacher EA, and Bernstein RE. 2006. Spectrophotometric measurements of pH in-situ: Laboratory and field evaluations of instrumental performance. *Environ. Sci. Technol. 40*(16), 5036-5044. doi:10.1021/es0601843.

Lloyd D, Thomas K, Price D, O'Neil B, Oliver K, and Williams TN. 1996. A membrane-inlet mass spectrometer miniprobe for the direct simultaneous measurement of multiple gas species with spatial resolution of 1 mm. *J. Microbiol. Methods 25*(2), 145-151. doi:10.1016/0167-7012(96)00011-5.

Lloyd D, Thomas KL, Benstead J, Davies KL, Lloyd SH, Arah JRM, and Stephen KD. 1998. Methanogenesis and CO2 exchange in an ombrotrophic peat bog. *Atmos. Environ. 32*(19), 3229-3238. doi:10.1016/S1352-2310(97)00481-0.

Lloyd D, Thomas KL, Cowie G, Tammam JD, and Williams AG. 2002. Direct interface of chemistry to microbiological systems: membrane inlet mass spectrometry. *J. Microbiol. Methods 48*(2-3), 289-302. doi:10.1016/S0167-7012(01)00331-1.

Martz TR, Carr JJ, French CR, and DeGrandpre MD. 2003. A submersible autonomous sensor for spectrophotometric pH measurements of natural waters. *Anal. Chem. 75*(8), 1844-1850. doi:10.1021/ac020568l.

Martz TR, Dickson AG, and DeGrandpre MD. 2006. Tracer monitored titrations: Measurement of total alkalinity. *Anal. Chem. 78*(6), 1817-1826. doi:10.1021/ac0516133.

Matz G, Kibelka GPG, Dahl J, and Lennemann F. 1999. Experimental study on solvent-less sample preparation methods: Membrane extraction with a sorbent interface, thermal membrane desorption application and purge-and-trap. *J. Chromatogr. A 830*(2), 365-376. doi:10.1016/S0021-9673(98)00853-X.

Mehrbach C, Culberson CH, Hawley JE, and Pytkowicz RM. 1973. Measurement of the apparent dissociation constants of carbonic acid in seawater at atmospheric pressure. *Limnol. Oceanogr. 18*(6), 897-907.

Millero FJ, and Leung WH. 1976. The thermodynamics of seawater at one atmosphere. *Am. J. Sci. 276*(9), 1035-1077.

Millero FJ. 2000. The activity coefficients of non-electrolytes in seawater. *Mar. Chem. 70*(1-3), 5-22.

Millero FJ. 2005. *Chemical Oceanography, Third Edition*. 3rd ed. CRC.

Millero FJ. 2007. The Marine Inorganic Carbon Cycle. *Chem. Rev. 107*(2), 308-341. doi:10.1021/cr0503557.

Monteiro P, Schuster U, Lenton A, Tilbrook B, Sabine C, Wanninkhof R, Takahashi T, Hood M, Olsen A, Bender M, et al. 2009. A global sea surface carbon observing system: assessment of changing sea surface CO2 and air-sea CO2 fluxes. In: *Community White Paper, OceanObs09*, Venice. Available from: http://www.oceanobs09.net/

Ørsnes H, Bohatka S, and Degn H. 1997. Reaction of water at hot filament interferes with measurements of dissolved gases by membrane inlet mass spectrometry. *Rapid Commun. Mass Spectrom. 11*(15), 1736-1738. doi:10.1002/(SICI)1097-0231(19971015)11:15<1736::AID-RCM50>3.0.CO;2-J.

Pasternak RA, J. F. Schimscheimer, and J. Heller. 1970. A dynamic approach to diffusion and permeation measurements. *J. Polym. Sci., Part A-2: Polym. Phys. 8*(3), 467-479. doi:10.1002/pol.1970.160080312.

Pilson ME. 1998. *Introduction to the Chemistry of the Sea, An*. 1st ed. Prentice Hall.

Precht E, Franke U, Polerecky L, and Huettel M. 2004. Oxygen dynamics in permeable sediments with wave-driven pore water exchange. *Limnol. Oceanogr. 49*(3), 693-705.

Randall M, and Failey CF. 1927. The activity coefficient of gases in aqueous salt solutions. *Chem. Rev. 4*(3), 271-284. doi:10.1021/cr60015a003.

Rao AM, McCarthy MJ, Gardner WS, and Jahnke RA. 2007. Respiration and denitrification in permeable continental shelf deposits on the South Atlantic Bight: Rates of carbon and nitrogen cycling from sediment column experiments. *Cont. Shelf Res. 27*(13), 1801-1819. doi:10.1016/j.csr.2007.03.001.

Rao AM, McCarthy MJ, Gardner WS, and Jahnke RA. 2008. Respiration and denitrification in permeable continental shelf deposits on the South Atlantic Bight: N2:Ar and isotope pairing measurements in sediment column experiments. *Cont. Shelf Res. 28*(4-5), 602-613. doi:10.1016/j.csr.2007.11.007.

Reimers CE, Girguis P, Stecher HA, Trender LM, Ryckelynck N, and Whaling P. 2006. Microbial fuel cell energy from an ocean cold seep. *Geobiology 4*, 123-136. doi:10.1111/j.1472-4669.2006.00071.x.

Royer JR, DeSimone JM, and Khan SA. 1999. Carbon dioxide-induced swelling of poly(dimethylsiloxane). *Macromolecules 32*(26), 8965-8973. doi:10.1021/ma9904518.

Sabine CL, Feely RA, Gruber N, Key RM, Lee K, Bullister JL, Wanninkhof R, Wong CS, Wallace DWR, Tilbrook B, et al. 2004. The oceanic sink for anthropogenic CO2. *Science 305*(5682), 367-371. doi:10.1126/science.1097403.

Salata GG, Roelke LA, and Cifuentes LA. 2000. A rapid and precise method for measuring stable carbon isotope ratios of dissolved inorganic carbon. *Mar. Chem. 69*(1-2), 153-161. doi:10.1016/S0304-4203(99)00102-4.

Sansone F, and Martens C. 1981. Methane Production from Acetate and Associated Methane Fluxes from Anoxic Coastal Sediments. *Science 211*(4483), 707-709. doi:10.1126/science.211.4483.707.

Sansone FJ, Spalding HL, and Smith CM. 2008. Submersible-operated porewater sampler for permeable sediments. *Limnol. Oceanogr.: Methods 6*, 119-125.

Sayles F, and Eck C. 2009. An autonomous instrument for time series analysis of TCO2 from oceanographic moorings. *Deep Sea Res. Part I 56*(9), 1590-1603. doi:10.1016/j.dsr.2009.04.006.

Schlüter M, and Gentz T. 2008. Application of membrane inlet mass spectrometry for online and in situ analysis of methane in aquatic environments. *J. Am. Soc. Mass. Spectrom. 19*(10), 1395-1402. doi:10.1016/j.jasms.2008.07.021.

Scholes RJ, Monteiro PMS, Sabine CL, and Canadell JG. 2009. Systematic long-term observations of the global carbon cycle. *Trends Ecol. Evol. (Amst.) 24*(8), 427-430. doi:10.1016/j.tree.2009.03.006.

Sheppard SK, and Lloyd D. 2002. Direct mass spectrometric measurement of gases in soil monoliths. *J. Microbiol. Methods 50*(2), 175-188. doi:10.1016/S0167-7012(02)00025-8.

Sheppard S, Gray N, Head I, and Lloyd D. 2005. The impact of sludge amendment on gas dynamics in an upland soil: monitored by membrane inlet mass spectrometry. *Bioresour. Technol. 96*(10), 1103-1115. doi:10.1016/j.biortech.2004.10.006.

Short R, Fries DP, Kerr ML, Lembke CE, Toler SK, and Byrne RH. 2001. Underwater mass spectrometers for in situ chemical analysis of the hydrosphere. *J. Am. Soc. Mass. Spectrom. 12*(6), 676-682. doi:10.1016/S1044-0305(01)00246-X.

Short RT, Fries DP, Toler SK, Lembke CE, and Byrne RH. 1999. Development of an underwater mass-spectrometry system for in situ chemical analysis. *Meas. Sci. Technol. 10*, 1195-1201.

Short RT, Toler SK, Kibelka GPG, Rueda Roa DT, Bell RJ, and Byrne RH. 2006. Detection and quantification of chemical plumes using a portable underwater membrane introduction mass spectrometer. *TrAC, Trends Anal. Chem. 25*(7), 637-646. doi:10.1016/j.trac.2006.05.002.

Smith T, Laursen A, and Deacon J. 2008. Nitrogen attenuation in the Connecticut River, northeastern USA; a comparison of mass balance and N2 production modeling approaches. *Biogeochemistry 87*(3), 311-323. doi:10.1007/s10533-008-9186-7.

Squillace PJ, Moran MJ, Lapham WW, Price CV, Clawges RM, and Zogorski JS. 1999. Volatile organic compounds in untreated ambient groundwater of the United States, 1985−1995. *Environ. Sci. Technol. 33*(23), 4176-4187. doi:10.1021/es990234m.

Sysoev AA. 2000. A mathematical model for kinetic study of analyte permeation from both liquid and gas phases through hollow fiber membranes into vacuum. *Anal. Chem. 72*(17), 4221-4229. doi:10.1021/ac991388n.

Taillefert M, Luther III GW, and Nuzzio DB. 2000. The application of electrochemical tools for in situ measurements in aquatic systems. *Electroanal. 12*(6), 401-412. doi:10.1002/(SICI)1521-4109(20000401)12:6<401::AID-ELAN401>3.0.CO;2-U.

Taylor S, and Bierbaum VM. 2008. Focus on Harsh Environment Mass Spectrometry. *J. Am. Soc. Mass. Spectrom. 19*(10), 1375-1376. doi:10.1016/j.jasms.2008.08.011.

Thompson AJ, Creba AS, Ferguson RM, Krogh ET, and Gill CG. 2006. A coaxially heated membrane introduction mass spectrometry interface for the rapid and sensitive on-line measurement of volatile and semi-volatile organic contaminants in air and water at parts-per-trillion levels. *Rapid Commun. Mass Spectrom. 20*(13), 2000-2008. doi:10.1002/rcm.2551.

Tortell P. 2005. Dissolved gas measurements in oceanic waters made by membrane inlet mass spectrometry. *Limnol. Oceanogr.: Methods 3*, 24-37.

de Vos Petersen C, Beck H, and Lauritsen F. 2004. On-line monitoring of important organoleptic methyl-branched aldehydes during batch fermentation of starter culture Staphylococcus xylosus reveal new insight into their production in a model fermentation. *Biotechnol. Bioeng. 85*(3), 298-305. doi:10.1002/bit.10885.

Watson J, and Payne P. 1990. A study of organic compound pervaporation through silicone rubber. *J. Membr. Sci. 49*(2), 171-205. doi:10.1016/S0376-7388(00)80786-3.

Weiss R. 1970. The solubility of nitrogen, oxygen and argon in water and seawater. *Deep Sea Res. 17*, 721-735.

Weiss R. 1974. Carbon dioxide in water and seawater: the solubility of a non-ideal gas. *Mar. Chem. 2*(3), 203-215. doi:10.1016/0304-4203(74)90015-2.

Wiesenburg DA, and Guinasso NL. 1979. Equilibrium solubilities of methane, carbon monoxide, and hydrogen in water and sea water. *J. Chem. Eng. Data 24*(4), 356-360. doi:10.1021/je60083a006.

Wijmans JG. 2004. The role of permeant molar volume in the solution-diffusion model transport equations. *J. Membr. Sci. 237*(1-2), 39-50. doi:10.1016/j.memsci.2004.02.028.

Woldring S. 1970. Biomedical application of mass spectrometry for monitoring partial pressures. A technical review. *J. Assoc. Adv. Med. Instrum. 4*(2), 43-56.

Yang TH, Wittmann C, and Heinzle E. 2003. Dynamic calibration and dissolved gas analysis using membrane inlet mass spectrometry for the quantification of cell respiration. *Rapid Commun. Mass Spectrom. 17*(24), 2721-2731. doi:10.1002/rcm.1251.

Yao W, and Byrne RH. 1998. Simplified seawater alkalinity analysis: Use of linear array spectrometers. *Deep Sea Res. Part I 45*(8), 1383-1392. doi:10.1016/S0967-0637(98)00018-1.

Appendices

Appendix 1: Instrument Specifications

Table 6. Underwater mass spectrometer system specifications.

Parameter	Specification
Mass Analyzer Type	Linear Quadrupole Mass Filter
Mass Range	1-200 amu
Inlet System	Membrane Introduction (PDMS)
Power Consumption	~100 Watts
Operation Voltage	24 VDC or 120 VAC
Maximum Deployment Time	10-14 Days (exhaust limited)
Dimensions	Diameter 19 cm, Length 114 cm
Weight	33 kg
Depth Capability	1000 m (extendable to >2000 m)

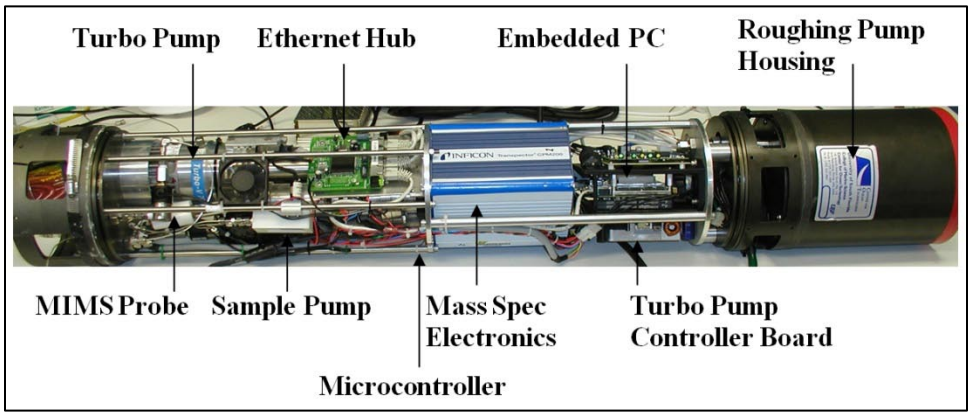

Figure 22. System level image of the underwater mass spectrometer.

Appendix 2: Instrument Response to Salinity

Raw instrumental data corresponding to instrument response with respect to salinity is shown in Figure 20. Triplicate subsamples obtained at 1.27 atm absolute and 184 atm absolute hydrostatic pressure show changes in gas fluxes with changing ionic strength (μ). Samples had identical fugacities that were generated by equilibrating NaCl solutions with a known gas mixture at a constant temperature. Dissolved gas concentrations can be calculated for comparison using the solubility equations of Weiss (1974) and Hamme and Emerson (2004). Samples were acidified to pH = 2, sample temperatures were 23.5 °C and membrane temperature was 35.0 °C. The gas mixture contained 990 ppm pCO_2^{dry} and 1% Ar.

Table 7. Baseline subtracted ion current data for argon (I_{40}) and carbon dioxide (I_{44}).

μ (μmol/kg-H_2O)	I_{40} (nA) 1.27 atm	I_{40} (nA) 184 atm	I_{44} (nA) 1.27 atm	I_{44} (nA) 184 atm
0.0	3.17, 3.10, 3.11	0.600, 0.598, 0.599	3.16, 3.16, 3.12	0.451, 0.456, 0.457
0.16	3.11, 3.09, 3.05	0.587, 0.591, 0.593	3.18, 3.14, 3.13	0.444, 0.453, 0.456
0.32	3.10, 3.00, 2.97	0.583, 0.597, 0.591	3.15, 3.11, 3.08	0.444, 0.455, 0.465
0.48	2.89, 3.00, 2.87	0.582, 0.586, 0.578	3.03, 3.10, 3.04	0.448, 0.447, 0.450
0.64	2.80, 2.77	0.570, 0.577, 0.574	3.03, 2.99	0.432, 0.449, 0.454
0.67(CRM)	2.80, 2.76, 2.79	0.573, 0.575, 0.571	2.98, 2.98, 2.97	0.445, 0.450, 0.443
0.72	2.73, 2.72, 2.78	0.573, 0.574, 0.568	2.95, 2.96, 3.02	0.445, 0.453, 0.451

About the Author

Ryan Bell received a Bachelor's of Science in Chemistry and Oceanography at the University of British Columbia in 2002. The first two years there Ryan focused on Geology and Earth Sciences. Ryan fondly remembers spending his summer months in northern British Columbia planting trees.

In 2002 Ryan moved to St. Petersburg, FL to begin his Master's in Marine Science at the University of South Florida. Enjoying his project developing underwater mass spectrometers, he soon entered the Ph.D. program. His first two years Ryan was financially supported by the von Rosenstiel Fellowship and the C.W. "Bill" Young Fellowship. Thereafter financial support came by way of employment by the University of South Florida's Center for Ocean Technology and SRI International. Working at these institutes has afforded Ryan many positive professional opportunities such as cruises, conferences, publications and workshops.